Unusual chemical bond and spectrum of beryllium dimer in ground $X^1\Sigma_g^+$ state

A. V. Mitin,[1, 2] A. A. Gusev,[3, 4] O. Chuluunbaatar,[3, 5] S. I. Vinitsky,[3, 6] V. L. Derbov,[7] and Luong Le Hai[8]

[1]*Moscow Institute of Physics and Technology, 9 Institutskiy per., Dolgoprudny, Moscow Region, 141700, Russia*[a]

[2]*Joint Institute for High Temperatures of RAS, Izhorskaya st. 13 Bd.2, 125412 Moscow, Russia*

[3]*Joint Institute for Nuclear Research, Dubna, Russia*[b]

[4]*Dubna State University, Dubna, Russia*

[5]*Institute of Mathematics and Digital Technology, Mongolian Academy of Sciences, 13330 Ulaanbaatar, Mongolia*[c]

[6]*Peoples' Friendship University of Russia (RUDN University), 117198 Moscow, Russia*[d]

[7]*N.G. Chernyshevsky Saratov National Research State University, Saratov, Russia*[e]

[8]*Ho Chi Minh City University of Education, Ho Chi Minh City, Vietnam*[f]

(Dated: 14 November 2023)

This review outlines the main results which lead to understanding the dual nature of the chemical bond in diatomic beryllium molecule in the ground $X^1\Sigma_g^+$ state. It has been shown that the beryllium atoms are covalently bound at low-lying vibrational energy levels ($v = 0 - 4$), while at higher ones ($v = 5 - 11$) they are bound by van der Waals forces near the right turning points. High precision *ab initio* quantum mechanical calculations of Be_2 resulted in the development of the modified expanded Morse oscillator potential function which contains all twelve vibrational energy levels [A.V. Mitin, Chem. Phys. Lett. 682, 30 (2017)]. The dual nature of chemical bond in Be_2 is evidenced as a sharp corner on the attractive branch of the ground state potential curve. Moreover, it has been found that the Douglas-Kroll-Hess relativistic corrections also show a sharp corner when presented in dependence on the internuclear separation. The difference in energy between the extrapolated and calculated multi-reference configuration interaction energies in dependence on the internuclear separation also exhibits singular point in the same region. The other problems of *ab initio* quantum mechanical calculations of the beryllium dimer are also discussed. Calculated spectrum of vibrational-rotational bound states and new metastable states of the beryllium dimer in the ground $X^1\Sigma_g^+$ state important for laser spectroscopy are presented. The vibration problem was solved for the modified expanded Morse oscillator potential function and for the potential function obtained with Slater-type orbitals [M. Lesiuk et al, Chem. Theory Comput. 15, 2470 (2019)]. The theoretical *upper and lower estimates* of the spectrum of vibrational-rotational bound states and the spectrum of rotational-vibrational metastable states with complex-valued energy eigenvalues and the scattering length in the beryllium dimer are presented.

———————

[a]Electronic mail: mitin.av@mipt.ru.

[b]Electronic mail: gooseff@jinr.ru

[c]Electronic mail: chuka@jinr.ru

[d]Electronic mail: vinitsky@theor.jinr.ru.

[e]Electronic mail: derbovvl@gmail.com

[f]Electronic mail: llhai611987@gmail.com

I. INTRODUCTION

The ground $X^1\Sigma_g^+$ state of the Be_2 molecule arises from the interaction of two singlet states, which corresponds to the closed shells of the Be atoms. Such a case occurs very rarely in diatomic molecules, which, however, is attractive from the theoretical point of view. The *ab initio* quantum mechanical calculations of such molecular ground states become significantly simple in comparison with other cases due to the simplification of the configuration state functions (CSF). This fact, together with the small number of electrons has led to numerous quantum mechanical calculations of the ground state of the Be_2 molecule being performed beginning with the 30s of the 20th century[1]. Subsequent investigations were reviewed in work[2]. The potential energy curve of the ground state of the Be_2 molecule, calculated and presented in publications[2–5], for the first time explicitly shows the complicated character of the chemical bonding in Be_2. The potential curve has a sharp corner at an internuclear distance of around 3.3 Å. This has been explained in 2009, both experimentally[6] and theoretically[7] (the last article was submitted for publication in November 2009 and published online in August 2010). Almost all vibrational energy levels of the ground state were determined in the experimental work and the Birge-Sponer[8] dependence of $\Delta G_{v+1/2} = E_{v+1} - E_v$ as a function of the vibrational quantum number v was obtained. This dependence shows different slopes of $\Delta G_{v+1/2}$ for the first five and for the upper vibrational levels (see Figure 2 in work[6]). This means that the vibrational constants of these groups of levels are different. On the other hand, theoretical analysis of the leading configurations of the multi-reference configuration interaction (MRCI) wave function[7] shows that the chemical bonding in Be_2 can be classified as a covalent bond at the internuclear distances near the equilibrium point, while at larger distances it transforms to the van der Waals interaction. Such a transformation of the electron density, which is associated with a change of the type of chemical bonding in Be_2, has been visualized in publication[9].

The Be_2 molecule is, thus, the first with a variable type of chemical bond depending on the vibrational quantum number. In this connection, let us consider a few representative recent *ab initio* calculations of the dissociation energy of Be_2 together with the corresponding values obtained from experiments all of which are presented in Table I. An analysis of these results shows that the values of D_e are close to each

TABLE I. Dissociation energy D_e (in cm^{-1}) of the ground state $X^1\Sigma_g^+$ of the Be_2 molecule, calculated in a few selected recent publications. Errors are shown, if estimated originally.

Year	Basis	Method	D_e	Reference
2005	23s10p8d6f3g2h	Extended geminals	945 ± 15	Røggen, Veseth[10]
2007	aug-cc-pcvqz+bf	CCSD(T)+FCI/CBS	938.7 ± 15	Patkovski et al.[11]
2009	*ab initio*	morphed RPC	934.6	Patkowski et al.[12]
2010	aug-cc-pvqz	FCI/CBS/correl corr	911.7	Schmidt et al.[13]
2011	aug-cc-pv6z	CCSD(T)/FCI+corr	935.1 ± 10	Koput[14]
2014		DMRG	931.2	Sharma et al.[15]
2015	STO/atc-etcc-6	fc/ae FCI/CCSD(T)/CBS	929.0 ± 1.9	Lesiuk et al.[16]
2017	t-aug-ccpV6Z	MRCI/CBS	929.8	Mitin[9]
2018	aug-cc-pVQZ	CCSDTQ+corr	928.0 ± 1.9	Magoulas et al.[17]
2018	cc-pV6Z	FCI/CBS+corr	922.9 ± 1.9	Rolik et al.[18]
2019	STO/atc-etcc-6	FCI/CBS+corr	934.6 ± 2.5	Lesiuk et al.[19]
2009	Experiment	EMO	929.7 ± 2.0	Merrit et al.[6]
2014	Experiment	EMO	929.6	Meshkov et al.[20]
2014	Experiment	MLR	934.8	Meshkov et al.[20]
2017	Experiment	MEMO	929.7 ± 2.0	Mitin[9]

other when they were computed directly as a difference of the total energies at the equilibrium point and at the dissociation limit or determined as parameter D_e in the expanded Morse oscillator (EMO) potential

function, defined as[21]:

$$V(r) = D_e[1 - e^{-\phi(r)(r-r_e)}]^2 \, , \tag{1}$$

$$\phi(r) = \sum_{i=0}^{n} \phi_i \left(\frac{r^p - r_{ref}^p}{r^p + r_{ref}^p} \right)^i \, , \tag{2}$$

which is used for approximation of the vibrational energy levels or points of the potential curve. Two alternate values of D_e predominate in these results: values of D_e of about 930 cm^{-1} were obtained in publications[6,9,15–17,20]. On the other hand, values of about 935 cm^{-1} have been obtained when the approximated potential functions, for example EMO, were corrected by the addition of the long-range asymptotic correction in the form of inverse-power terms and were used for fitting the experimental energy levels or the calculated theoretical points of a potential curve. This was the case in works[12,19,20]. It is especially important to note that the values of D_e equaling 929.6 and 934.8 cm^{-1} were obtained in work[20] when the same experimentally determined vibration energy levels were approximated by using EMO and Morse long-range (MLR) potential functions, i.e. without a correction for long range asymptotic behavior and with it. Additionally, in the same article, the experimental energy levels were fitted using the Chebyshev polynomial expansion (CPE) function. In general, the use of orthogonal polynomials, including Legendre and Chebyhev polynomials of the first and the second kind, for the approximation of a potential curve by the optimal approximating polynomial was proposed in works[22,23]. These three types of polynomials permit the assignment of different weights for approximated points, which might be useful for accounting for variable experimental measurement errors more correctly.

The inconsistency in the values of D_e determined by the different ways mentioned above can be understand by considering the approximation methods employed for the determination of the corresponding potential curves. They are usually defined by minimizing the root mean square (RMS) deviation of the optimized potential curve from the *ab initio* calculated points or similarly by minimizing the RMS deviation of the calculated vibrational energy levels from the measured ones. Thus, the values of D_e in the different formulas of potential curves are defined in a such way to give the minimum RMS for different formulas. Therefore, from the approximation theory follows that the D_e is just a parameter, which values have to be differ in different formulas and its value can not be compared from the different formulas. Obviously, this case shows a problem of inconsistency between physics and mathematics, because D_e is considered as a dissociation energy in physics. Although, it is well known that the dissociation energies can not be directly experimentally measured and D_0 can only be approximately estimated from the rotational vibrational spectra[24].

The dual nature of the chemical bonding in Be$_2$ is evident in the calculations of the vibrational energy levels of the ground state with the EMO potential function. The transition to the twelfth vibration level, which was clearly observed in the spectrum, has not been identified in the experimental work[6]. This happens because the EMO potential function used to calculate the vibrational energy levels in Be$_2$ holds only eleven energy levels. However, the EMO potential function was originally proposed for the description of the covalent chemical bond. On the other hand the van der Waals bond is weaker and more important for larger internuclear distances in comparison to the covalent bond. For this reason, it is clear that the EMO potential function of Be$_2$ is more narrow near dissociation limit in comparison with the correct one, which has to describe the van der Waals interaction at large distances in Be$_2$. This was noted first in work[12]. Later, this problem of the EMO potential function[6] was corrected in the modified EMO (MEMO) potential function by including the *ab initio* MRCI potential near the dissociation limit in the EMO potential function[9]. The MEMO potential function, constructed in such a way, holds all twelve vibrational energy levels of Be$_2$.

An important question follows from the dual nature of the chemical bond in the Be$_2$ molecule. Most of the available Gaussian basis sets for *ab initio* calculations were developed for the description of the covalent and ionic type of bonding. However, due to the dual nature of the chemical bond in Be$_2$, the

basis set used in *ab initio* calculations have to describe both covalent bonding in the vicinity of equilibrium distance and van der Waals bonding at large distances at the same level of quality.

The significance of this problem can be demonstrated by considering the convergence of the calculated results depending on the size of the employed basis sets, i.e. the number of basis functions. In this connection, a few large Gaussian basis sets have been developed and used in extended quasi-relativistic MRCI calculations of the dissociation energy D_e of the Be_2 molecule. This energy was estimated as a difference of the total energies computed at point near the equilibrium and at point corresponding to the dissociation limit, i.e. at $R = 2.44$ and $R = 80.0$ Å, correspondingly. For the first time, the dependence of D_e on the basis set size is given in Table II. The presented values of D_e were corrected for the basis set superposition error (BSSE).

TABLE II. Dissociation energies D_e (in cm^{-1}) of the ground state $X^1\Sigma_g^+$ of Be_2 calculated using the MRCI method together with the corresponding basis sets and the number of CSF used in calculation.

Basis	CSF	D_e
(16s10p5d4f3g2h1i)/[7s6p5d4f3g2h1i]+(3s3p3d3f3g3h3i)	200 073 854	948.8
(18s12p5d4f3g2h1i)/[8s7p5d4f3g2h1i]+(3s3p3d3f3g3h3i)	203 636 850	937.7
(18s12p6d5f4g3h2i)/[8s7p6d5f4g3h2i]+(3s3p3d3f3g3h3i)	217 677 644	934.0
(20s14p6d5f4g3h2i)/[9s8p6d5f4g3h2i]+(3s3p3d3f3g3h3i)	242 592 786	930.4
(22s16p6d5f4g3h2i)/[10s9p6d5f4g3h2i]+(3s3p3d3f3g3h3i)	246 197 719	928.0

It is well known that the contribution of the van der Waals interaction to D_e is smaller in comparison with the covalent one. In this connection it is reasonable to assume that the correlation energy corresponding to the van der Waals interaction converge to their limit faster with increasing of the number od basis functions and CSF in comparison with that for the covalent interaction. The results presented in this Table II shows that the D_e reduces from over 935 to below 929.6 cm^{-1}, which is the lowest experimental value of Be_2 dissociation energy. Hence, one can conclude that the fraction of correlation energy which was taken into account in the calculations presented in this table reduces with increasing the number of basis functions despite of small enlarging the number of CSF. Therefore, an equivalent description of the van der Waals and covalent bonding in Be_2 was not reached in these calculations despite large number of CSFs included in the MRCI calculations[25].

It should be noted that quantum mechanical *ab initio* calculations are based on the statement that the obtained results must converge to the correct ones when increasing the number of employed basis functions and CSFs. It is well known that all published *ab initio* calculations of Be_2 were only performed with a single selected basis set (or with two sets when extrapolation to the infinite number of basis functions was employed). This means that a good agreement in some publications between the calculated D_e and the experimental ones must be considered just as a lucky case.

II. *AB INITIO* CALCULATIONS OF BE$_2$ AND MODIFIED EMO POTENTIAL ENERGY FUNCTION

In the light of the comments presented above, the MRCI calculation of the potential curve of the ground $X^1\Sigma_g^+$ state of the Be_2 molecule given in publication[9] looks like a compromise in accounting for the outlined problems which, however, reproduce the experimental dissociation energy D_e well.

High-precision *ab initio* MRCI calculations of the Be_2 potential curve have been performed using a well known program[26] with correlation consistent cc-pVQZ and cc-PV5Z basis sets[27], extended by four augmented functions[28,29] for the better description of the van der Waals interaction. Molecular orbitals obtained in the Hartree-Fock calculations were transformed into pseudo-natural orbitals to improve convergence of the configuration expansion set. Relativistic effects have been taken into account using the Douglas-Kroll-Hess approach[30–32]. The calculated total electronic energies have been corrected using the Boys-Bernardi counterpoise method[33] to eliminate the BSSE[34] and then were extrapolated to the infinite basis set for the case of using natural orbitals in accordance with the considerations given in work[35]. The

scalar relativistic corrections and application of extrapolation to the infinite basis set in the Be_2 molecule were investigated in Refs.[3,7,14,19,36]. The total many configuration molecular wave function for the largest MRCI calculation of Be_2 was constructed from the list of reference configurations consists of a complete active space of about $1.6 \cdot 10^4$ configurations formed by 24 molecular orbitals of D_{2h} symmetry, which describe the excitations of electrons to the $2p$, $3s$, $3p$, and higher orbitals of Be. All singly and doubly excited configurations generated from this list of reference configurations have been included in the MRCI calculations. The largest calculation includes about $37.2 \cdot 10^6$ configuration state functions.

The values of the total potential energy of Be_2 calculated at 77 points of internuclear separation obtained in these calculations are presented in Table III. A comparison of the theoretical potential energy

TABLE III. MRCI potential energy curve of the $X^1\Sigma_g^+$ state of Be_2. Internuclear separation is in angstrom (Å), the total energy is in (cm^{-1}).

R	E_{tot}	R	E_{tot}	R	E_{tot}	R	E_{tot}
1.50	24554.9792	3.00	-478.4235	6.00	-29.8545	24.00	-0.0275
1.60	16238.9043	3.10	-415.5393	6.50	-17.9725	25.00	-0.0250
1.70	10237.2474	3.20	-366.2914	7.00	-11.1156	26.00	-0.0250
1.80	6045.0232	3.30	-328.1793	7.50	-7.0865	27.00	-0.0217
1.90	3201.9108	3.40	-298.4670	8.00	-4.6482	28.00	-0.0136
2.00	1344.4657	3.50	-274.7081	9.00	-2.1839	29.00	-0.0141
2.10	192.0413	3.60	-254.8773	10.00	-1.1249	30.00	-0.0089
2.20	-469.1904	3.70	-237.3498	11.00	-0.6198	32.00	-0.0160
2.30	-800.1700	3.80	-220.9879	12.00	-0.3804	34.00	-0.0099
2.40	-920.4464	3.90	-205.7910	13.00	-0.2399	36.00	-0.0086
2.42	-927.3053	4.00	-192.2289	14.00	-0.1588	38.00	-0.0062
2.43	-929.0688	4.20	-167.4891	15.00	-0.1080	40.00	-0.0072
2.44	-929.8058	4.40	-143.7740	16.00	-0.0818	42.00	-0.0052
2.45	-929.5907	4.60	-121.5195	17.00	-0.0658	44.00	-0.0030
2.46	-928.4713	4.80	-101.3230	18.00	-0.0448	46.00	-0.0028
2.50	-916.0723	5.00	-83.5874	19.00	-0.0395	48.00	-0.0026
2.60	-846.1587	5.20	-68.4332	20.00	-0.0318	50.00	0.0000
2.70	-749.2164	5.40	-55.7499	21.00	-0.0227		
2.80	-648.4697	5.60	-45.2901	22.00	-0.0262		
2.90	-556.4006	5.80	-36.7651	23.00	-0.0343		

function given in this table with the EMO potential function derived from fitting the experimental energy levels shows that, near the equilibrium point, the EMO function is broader compared with the theoretical potential energy function. However, the EMO function is narrower in comparison to the theoretical one near the dissociation limit, which is expected in light of the above analysis. For this reason, the EMO potential function has only eleven vibration levels, while the twelfth energy level is pushed out to the continuum spectrum.

From this analysis follows that the EMO potential function derived from the experimental results can be improved by modifying its part near dissociation limit. Following this conclusion, the modified MEMO potential function was constructed by replacing the repulsive branch of the EMO potential function above the dissociation limit and its attractive branch above 895 cm^{-1} with the theoretical counterparts.

The parameters of the MEMO potential function obtained in such a way and the corresponding vibrational energy levels are given in Table IV. The values of the vibrational energy levels calculated with other published potentials, where all twelve vibration energy levels were obtained, are also given in this table. A comparison of the EMO and MEMO potential functions shows that the modified function has all twelve vibrational levels and better describes the experimental vibrational energy levels due to smaller RMS error. The twelfth level of MEMO potential has three rotational levels with $J = 0, 1, 2$ which are about 0.3 cm^{-1} below the dissociation limit.

The *ab initio* potentials presented in publications[12,14] have RMS errors of about 0.1 and 0.3 cm^{-1},

TABLE IV. Spectroscopic parameters of the Be$_2$ molecule. Vibration energy levels are in cm^{-1}, R_e is given in Å.

	MRCI	MEMO	MEMO*	MRCI	MRACPF	SAPT	CV+F+R +corr	CCSDTQ +corr	FCI/CBS RPC	STO*	morphed	MRL	EMO	Exp
Ref.	9	9	37	5	38	12	14	17	19	37	12	20	6	6
R_e	2.4427	2.4535	2.45534	2.4485	2.4443	2.443	2.434	2.4344	2.4436	2.447	2.445	2.438	2.4536	
D_e	929.84	929.74	929.8	893	898±8	938.7	935.1±10	928.0	934.6±2.5	934.4	934.6	934.8	929.74	929.7±2.0
D_0	802.59	806.5	806.0	768.2	772.2		808.3	798.5	807.7	807.7		808.2	806.5	807.4
G(0)	127.2	123.3	123.7	124.8	125.8		126.8	129.5		126.6		126.7		
G(1)-G(0)	224.0	222.2	222.5	218.4	218.6	222.3	222.7	227.4	223.4	223.5	222.6	222.9	222.7	222.6
G(2)-G(0)	400.3	397.6	397.3	387.0	388.1	397.6	396.8	405.1	400.1	398.2	397.0	397.4	397.8	397.1
G(3)-G(0)	523.0	517.9	517.7	499.0	503.2	520.3	517.8	526.0	517.3	519.3	518.2	518.4	518.2	518.1
G(4)-G(0)	600.1	595.1	594.8	568.0	576.0	597.9	594.7	598.5	595.1	595.7	594.8	595.1	595.4	594.8
G(5)-G(0)	655.9	652.1	651.9	622.4	631.0	655.1	651.6	652.6	651.7	652.2	651.5	651.8	652.4	651.5
G(6)-G(0)	701.1	699.1	698.9	668.5	676.2	702.6	698.9	697.9	698.7	699.3	698.7	699.0	699.4	698.8
G(7)-G(0)	738.7	738.0	737.7	706.1	712.4	741.7	738.0	735.3	738.0	738.1	737.6	738.0	738.2	737.7
G(8)-G(0)	767.9	768.6	768.2	734.8	740.0	772.4	768.6	764.1	768.3	768.6	768.2	768.5	768.8	768.2
G(9)-G(0)	788.0	790.0	789.7	754.2	758.9	794.3	790.4	783.9	790.1	790.1	790.0	790.2	790.7	789.9
G(10)-G(0)	799.0	802.1	801.6	764.6	769.0	807.1	803.1	794.8	802.6	802.6	802.5	802.8	803.4	802.6
G(11)-G(0)	802.4	806.2	805.7	768.0	772.0	811.9	807.9	798.2	807.5	807.2	807.1	807.6		
RMS	3.1	<0.4	<0.4	25.7	22.6	3.4	0.3		1.0	0.7	< 0.1	0.3	0.6	

TABLE V. Deviations of the calculated vibrational energy levels from the experimental ones $(E(exp) - E(calc))$ for different vibration number v in cm^{-1}.

v / Ref.	morphed RPC [12]	CV+F+R [14]	FCI/CBS +corr [19]	STO* [37]	MEMO [9]	MEMO* [37]
1	0.0	-0.1	-0.8	-0.9	0.4	0.1
2	0.1	0.3	-3.0	-1.1	-0.5	-0.2
3	-0.1	0.3	0.8	-1.2	0.2	0.4
4	0.0	0.1	-0.3	-0.9	-0.3	0.0
5	0.0	-0.1	-0.2	-0.7	-0.6	-0.4
6	0.1	-0.1	0.1	-0.5	-0.3	-0.1
7	0.1	-0.3	-0.3	-0.4	-0.3	0.0
8	0.0	-0.4	-0.1	-0.4	-0.4	0.0
9	-0.1	-0.5	-0.2	-0.2	-0.1	0.2
10	0.1	-0.5	0.0	0.0	0.5	1.0

correspondingly, while the potential obtained in work[19] has a somewhat larger RMS error of about 1.0 cm^{-1}. The values of D_e for these three potentials, equal to 934.6, 935.1 and 934.6 cm^{-1}, are close to each other. Although, only for the second potential, D_e probably was estimated as the difference of the total energy at the equilibrium point and at the distance near dissociation limit, while for the first and third potentials D_e were determined by fitting the theoretical points calculated in limited regions by potentials, which takes into account long-range asymptotic corrections.

Other differences between potentials can be observed by comparing the deviations of calculated vibrational energies from the experimental ones presented in Table V. For the first potential, deviations are distributed approximately uniformly over the whole range of energy levels. For the second potential, the largest deviations are located close to the bottom and top of the vibrational energy spectrum, while for the third potential the largest deviations are observed only for low lying vibration energy levels. Such variations in the distributions of deviation errors can be explained as being the manifestation of the problem mentioned above: the equivalent description of the covalent and van der Waals chemical bonding in Be$_2$ by the basis set used in *ab initio* calculations. For comparison, for the MEMO potential the deviations are approximately uniformly spread over all energy levels just like for the first potential[12].

A comparison of the vibrational energy levels calculated for EMO/MEMO and MLR/CPE potentials shows that the main discrepancy between them arises from the different values of the zero vibrational energy level $G(0)$: 123.2 and 123.3 cm^{-1} for EMO/MEMO, while for MLR/CPE potentials the values of G(0) are 126.6 and 126.8 cm^{-1}, correspondingly. This difference gives the main contribution to the different values of D_e equal to 929.7 and 934.8 cm^{-1}, respectively. In general, the observed significant influence of the values of a potential at large distances on $G(0)$ is an unexpected result, which can not be easily explained. This is a problem for further investigations.

In this connection, note that the good agreement of the experimental value of $G(0)$ for MLR/CPE potentials with the theoretical one obtained in work[14] - 126.9 cm^{-1} can not be considered indicative of a correct result. This result was obtained using a basis set with contracted s and p functions, however when a basis set with with uncontracted s and p functions is used, as was done in work[5], a value of $G(0)$ of 124.8 cm^{-1} is obtained. This points out that the contraction of s and p functions in basis sets probably noticeably reduces the basis set flexibility in describing the potential near the minimum point.

Summarizing the above notes we can conclude that the MEMO and MLR potentials are the best ones among those derived from the experimental data, although the differences in value of $G(0)$ and D_e are now not explainable. Theoretical potentials presented in publications[12,14] stand out favorably from the known ones. Most importantly, however, special attention should be paid to comparing different forms of employed asymptotic corrected potentials.

III. CHEMICAL BONDING IN BERYLLIUM DIMER AND EXPERIMENTAL POTENTIAL ENERGY FUNCTION

The $X^1\Sigma_g^+$ ground state MEMO potential curve of Be_2, constructed in work[9], is presented on Figure 1 together with the calculated vibrational energy levels, designated by horizontal lines at corresponding energies. The figure shows that the slope of the attractive part of the potential curve changes after the fourth vibrational level, indicating the change of the character of the chemical bond in Be_2: having a predominantly covalent nature in the low part (shaded in gray), and a more strongly van der Waals bond for the higher vibrational levels. This means that the low-lying ($v = 0-4$) and upper vibrational energy levels can only be correctly described by two separate sets of Dunham coefficients[39,40], one of which is used for describing the low-lying levels and the other one for the upper ones, i.e. the fundamental vibration frequencies ω_e (Y_{10}), or force constants of these vibration levels, are different. As mentioned above, this fact has been experimentally shown in work[6], where the dependence of $\Delta G_{v+1/2} = E_{v+1} - E_v$ as a function of the vibrational quantum number v was constructed. Figure 2 in this reference displays different slopes of $\Delta G_{v+1/2}$ for the first five vibrational levels compared to the higher lying ones. This leads to the conclusion that the chemical bonding in Be_2 on the low-lying and upper vibrational energy levels are different. This conclusion has been confirmed by an investigation of the expansion coefficients of the MRCI wave functions, published in work[7], which shows that the distribution of the total electron density in Be_2 corresponds to the usual covalent interaction at low-lying vibrational levels near the equilibrium point. On the other hand, for the upper levels, near the right turning points, the total electron density distributions are described as two asymmetric ellipsoidal distributions (pointed at each other) of the electron densities centered on the positions of the nuclei. This type of total electron density distribution clearly corresponds to the van der Waals interaction.

In this connection, to show dual nature of chemical bonding in the beryllium dimer, the total electron densities of Be_2 were calculated in work[9] for internuclear separations corresponding to the right turning points of the vibrational levels $v = 2-6$ and are presented on Figure 2. This figure visualizes the successive transformation of the covalent bonding at the right turning points, which is realized in Be_2 on the low-lying vibrational levels $v = 0-4$, to the van der Waals bonding on the upper vibrational levels $v = 5-11$.

The transformation of the chemical bonding in Be_2 depending on the vibrational quantum number or the main configurations of the total molecular wave function depending on the internuclear separation should be evident in other physical characteristics of the molecule as well. In particular, the investigations of the relativistic corrections[30–32] as a function of the internuclear separation, presented in work[41], shows that this dependence also has a sharp turn indicated by arrow in the inset on Figure 1. The dependence of the difference of energies between the extrapolated MRCI and the MRCI energy obtained with the cc-pV5Z basis sets in dependence on the internuclear distance[41] presented on Figure 1 also has a specific point in the same region of the internuclear separations. This is especially interesting because only the energies obtained with two different basis sets are included in the formula of the employed extrapolation method[35].

In the experimental work[6], the dual nature of the chemical bond in Be_2 was overlooked. For this reason the usual EMO potential function has been employed by the authors for the description of the interaction potential in it. However, the Morse oscillator (MO) potential function introduced in work[42] and its generalization - expanded Morse oscillator EMO function[21] were proposed to describe covalent chemical bonds in molecules when the mutual attractive forces quickly decrease with increase of the internuclear distance. The exponential dependences of MO and EMO potential functions from the internuclear separations describe this type of chemical interaction well. Contrary to this case, the van der Waals interaction in molecules is described by a potential function whose potential well is usually significantly smaller and its depth reduces significantly slower in comparison with those of covalent bonding. The main asymptotic term with respect to the internuclear distance (R) of such a potential function is proportional to $1/R^6$. Therefore, the EMO potential function better describes covalent bonding rather than van der Waals bonding.
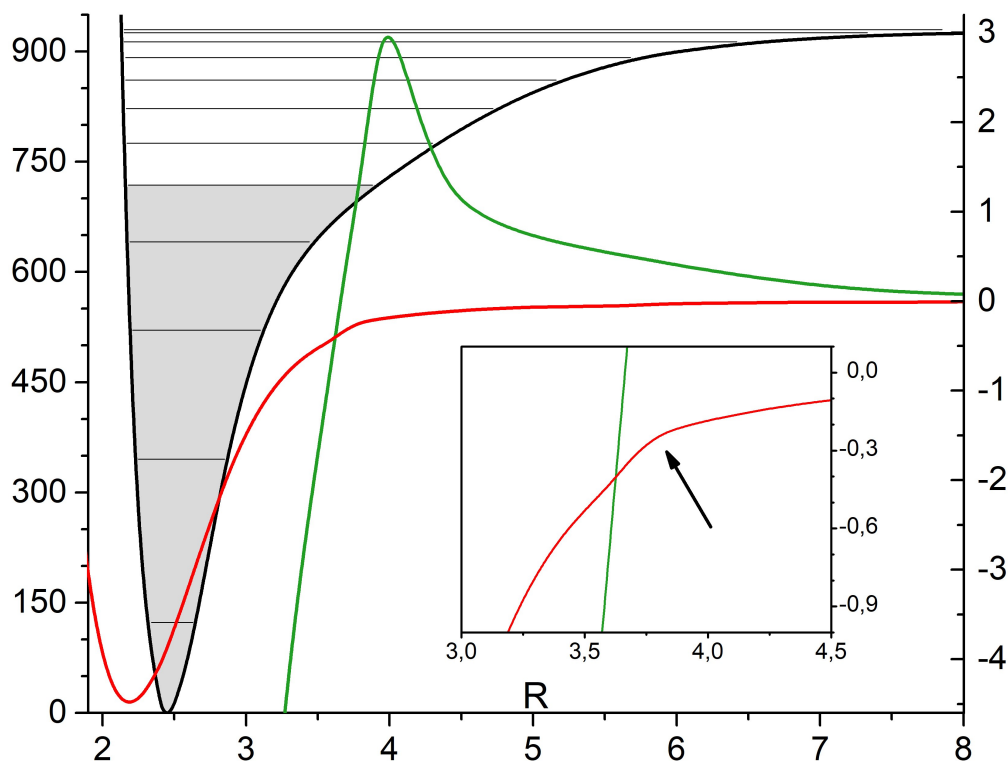
FIG. 1. The $X^1\Sigma_g^+$ ground state Be$_2$ MEMO potential energy curve together with the calculated vibrational energy levels (black) corresponding to the left vertical axis. The relativistic corrections (red) and the differences between extrapolated and calculated MRCI energies (green) corresponding to the right vertical axis as a function of the internuclear separation (R) given in Å. Energies are given in cm^{-1}.
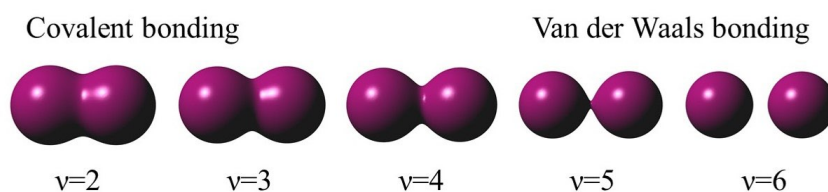

FIG. 2. The transformation of the total electron density isosurfaces for the Be$_2$ molecule at the right turning points for different vibrational quantum numbers v, showing the modification of the covalent bonding at low-lying v into the van der Waals one with increasing v.

Note, that in the article[12], published shortly after the experimental work[6] on Be$_2$, the authors noted that the problem with the assignment of the twelfth vibration energy level with v=11 could have arisen due to incorrect asymptotic behavior of the EMO potential function as internuclear distance increases beyond 5 Å. However, in publications[7,9] the argument has been made that the transformation of covalent bonding to the van der Waals one begins at a distance of about 3.3 Å. The results of *ab initio* calculations

presented in work[12] support this conclusion. The *ab initio* calculations of the Be_2 interaction potential were performed for 20 internuclear distances and the obtained points were fitted using a function with correct asymptotic behavior (eq. (1) in[12]). As a result, the twelve vibrational energy levels of this potential reproduce the experimental ones with an RMS error of 3.4 cm^{-1}. Comparing the calculated vibrational energy levels to the experimental values, presented in[12] shows that the deviations increase as one moves from the low-lying vibrational levels to the top ones. Such behavior of the deviations is, once again, reasonably explained by the fact that the basis set used in *ab initio* calculations was primarily developed for the description of covalent bonding and does not give an equivalent description of the van der Waals interaction at large internuclear separations. In this article, the semi-empirical "morphed" potentials has also been presented, which reproduces the experimental vibrational energy levels with an RMS error of less than 0.1 cm^{-1}.

IV.   THE POTENTIAL ENERGY CURVES AND ITS EXTENSION ON A LARGE INTERVAL

In quantum chemical calculations, the potential energy curves (PECs) of interatomic interaction are presented in the form of numerical tables calculated with limited accuracy and defined on a nonuniform mesh of nodes in a finite domain of interatomic distance variation. However, for a number of diatomic molecules the asymptotic expressions for the PEC are calculated analytically for sufficiently large distances between the atoms[45–47].

To formulate the boundary value problem (BVP) on a semiaxis, the PEC should be continued beyond the finite interval using additional information about the interaction of atoms comprising the diatomic molecule at large interatomic distances. The dominant term of the PEC at large distances is given by the van der Waals interaction, inversely proportional to the sixth power of the independent variable with the constant, determined from theory[43,44].

Proceeding in this way we faced a problem how to match smoothly the PEC asymptotic expansion with its tabulated numerical values (within the accuracy of their calculation) at a suitable sufficiently large distance and calculate correctly the required sets of bound, metastable and scattering states. We studied this problem and developed the procedure of approximating MEMO PEC[9] by Lagrange interpolation polynomials (LIPs) and its extension on large interval by means of the smooth matching procedure using Hermite interpolation polynomials (HIPs) preserving continuous derivative of the PEC in a matching point[48–50]. Constructing in such a way PEC was called MEMO*.

By this way we solved the above class of eigenvalue, metastable and scattering problems for the second-order ordinary differential equations[37] using the programs KANTBP 3.0[51] and KANTBP 5M [52],the updated version of KANTBP 4M[53], implementing the finite element method (FEM)[48,54] in Fortran and Maple, respectively.

The Schrödinger equation for a diatomic molecule in the adiabatic approximation (in which the diagonal nonadiabatic correction is not taken into account), commonly referred to as Born–Oppenheimer (BO) approximation, has the form[37]

$$\left(-s_2 \frac{1}{r^2}\frac{d}{dr}r^2\frac{d}{dr} + V_J(r) - E\right)\Phi_J(r) = 0, \tag{3}$$

$$V_J(r) = V(r) + s_2\frac{J(J+1)}{r^2}, \quad s_2 = \frac{\hbar^2}{2m}\frac{1}{\text{Å}^2}.$$

Here J is the total angular momentum quantum number, $m = M/2 = 4.506$ Da is the reduced mass of beryllium molecule expressed in 1 Da = 931.494061 MeV/c^2 atomic mass unit (u)[55], 1 eV = 8065.54429 cm^{-1}, $\hbar c = 1973.269718$ eV Å, and $\hbar^2/(2m) = 3.741151852 \cdot 10^{-8}$ Å. The factor $1/\text{Å}^2$ in s_2 means that the distance r between atoms is expressed in Å, and $s_2 = 3.741151852$ cm^{-1}. Also E is the energy in cm^{-1} and $V(r)$ is PEC in cm^{-1}.
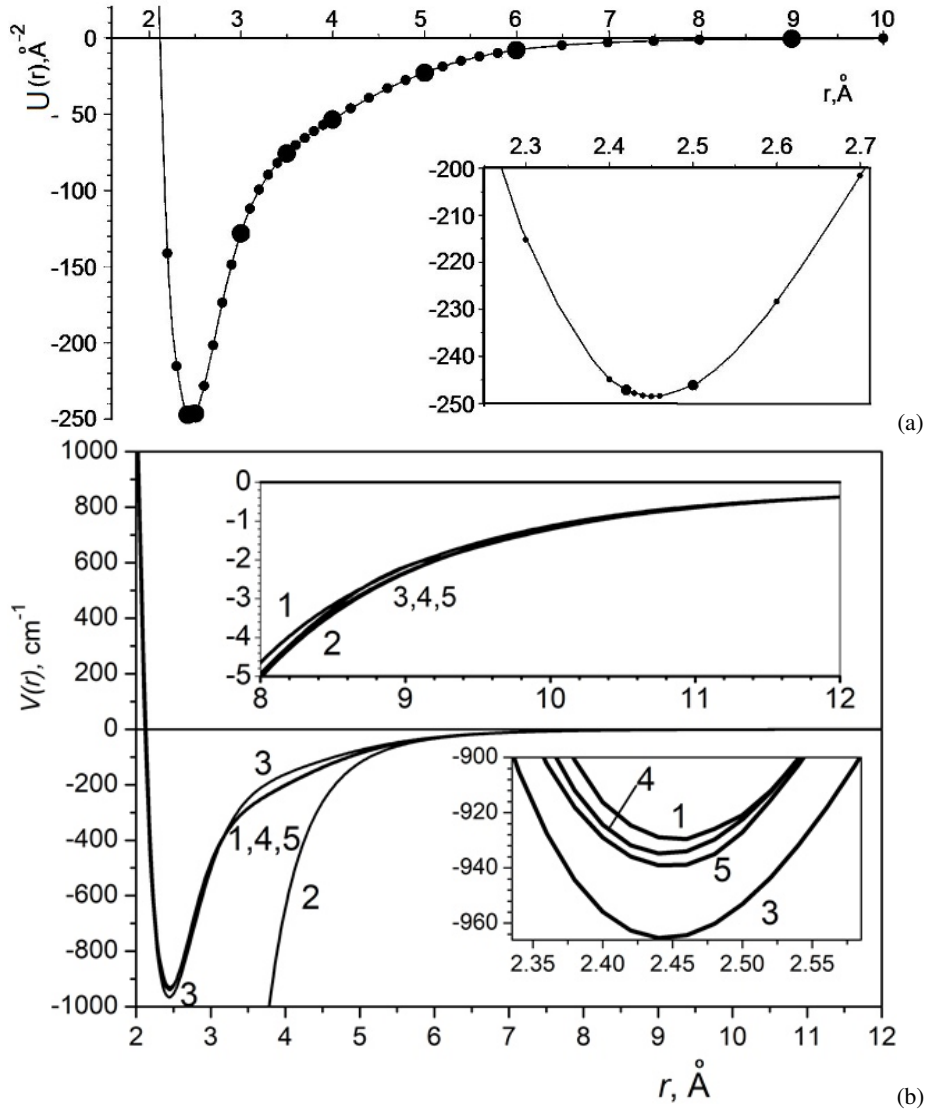
FIG. 3. (a) Potential $U(r)$ (Å^{-2}) of the beryllium dimer as a function of internuclear distance r (Å) obtained by interpolating the MEMO tabulated values[37] (points in the subintervals, the boundaries of which are shown by larger dots) by the fifth-order LIPs. (b) MEMO* potential $V(r)$ (points in (a) and line 1, Ref.[37]), the asymptotic expansion $V_{as}(r)$ of MEMO function (line 2, Ref.[43]), the analytical forms of the potential function $V_{an}(r)$ (line 3, Ref.[44], line 4, Ref.[19], and line 5, Ref.[20]). r is given in Å, $V(r)$ in cm^{-1}.

For the numerical calculations the potential, energy, and wave number in angstroms are used

$$U(r) = \frac{1}{s_2}V(r) \cdot \text{Å}^{-2}, \quad \bar{\mathscr{E}} = \mathscr{E} \cdot \text{Å}^{-2}, \quad \bar{k} = \sqrt{\bar{\mathscr{E}}} = \sqrt{\mathscr{E}} \cdot \text{Å}^{-1}, \tag{4}$$

where $\mathscr{E} = E/s_2$, and $k = \sqrt{\mathscr{E}}$ are the dimensionless energy and wave number.

In Ref. [37] the potential $V(r)$ (in cm^{-1}) is given by the MEMO* potential function which is an approximation of the MEMO tabular values $\{V(r_i)\}_{i=1}^{76}$ in interval $r \in [r_1 = 1.5, r_{76} = 48]$. Here and below, the
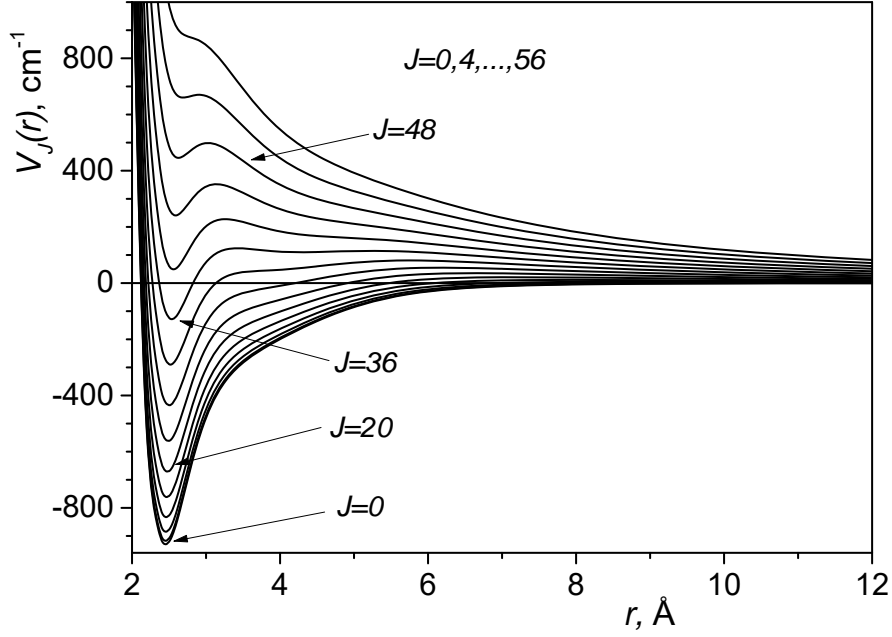
FIG. 4. MEMO* potential functions $V_J(r)$ at $J = 0, 4, 8, \ldots, 56$.

value r is given in units of Å unless otherwise is indicated. These tabular values were chosen to provide better approximation of the potential $V(r)$ by the fifth-order Lagrange interpolation polynomials (LIPs) of the variable r in subintervals $r \in [r_{5k-4}, r_{5k+1}]$, $k = 1, \ldots, 15$. Indeed, one can see that Figure 3 displays a smooth approximation till $r_{49} = 12$, where the approximate PEC is matched with the asymptotic potential $V_{as}^{BO}(r) = s_2 U_{as}^{BO}(r)$ given analytically by the expansions[43]

$$U_{as}^{BO}(r) = s_1 \tilde{V}_{as}^{BO}(r), \quad \tilde{V}_{as}^{BO}(r) = -\left(214Z^{-6} + 10230Z^{-8} + 504300Z^{-10}\right), \tag{5}$$

where $s_1 = aue/s_2 = 58664.99239$ or $s_1 s_2 = aue = 219474.6314 \text{ cm}^{-1}$, $Z = r/s_3$ and $s_3 = 0.52917$ is the Bohr radius in Å. This fact allows considering the interval $r \in [r_{match} \geq 12, \infty)$ as possible for using the asymptotic potential $V_{as}^{BO}(r)$ at large r and executing conventional calculations based on tabular values of $V(r)$ in the finite interval $r \in [r_1, r = 12]$ (see also[19]).

We note that the MEMO tabular values for $r \in \{r_{42} = 6.5, \ldots, r_{48} = 11\}$ are smaller than the asymptotic ones by $5.5 \div 6\%$, for $r = r_{51} = 14$ exceed the asymptotic ones by 8%, and beyond the interval $r \in [r_{41} = 6.0, \ldots, r_{52} = 15]$ the difference is more than 10%.

Based on this fact, the potential $V(r)$ in subintervals $r \in [r_{5k-4}, r_{5k+1}]$, $k = 1, \ldots, 9$ was approximated by the fifth-order Lagrange interpolation polynomials (LIPs) of the variable r in the interval $r \in [r_1, r_{46} = 9]$. In subinterval $r \in [r_{46} = 9, r_{match} = 14]$ we consider the approximation of the potential $V(r)$ by the fourth-order HIPs using the values of the potential $V(r)$ at the points $r = \{r_{46} = 9, r_{47} = 10, r_{48} = 11\}$ and the values of the asymptotic potential $V_{as}(r)$ and its derivative $dV_{as}(r)/dr$ at the point $r = r_{match} = 14$. In the interval $r \in [r_{match} = 14, \infty)$, the potential $V(r)$ is approximated by the asymptotic expansion (5). Let us emphasize that this approximation using the HIP provides a smooth matching of the interpolated values of the tabulated function with its asymptotic continuation, in particular case (5), in comparison with the conventional approximation by LIPs, which has no continuous derivative at a boundary of joined intervals[48]. Potentials $V_J(r)$ are displayed in Figure 4 at $J = 0, \ldots, 56$ with the step 4.

In Ref.[19], the potential $V(r)$ (in cm^{-1}) (see Figure 3) is given by the BO potential function plus relativistic potential function marked as STO with tabular values $\{V(Z_i)\}_{i=1}^{28}$ in the interval $Z \in [Z_1 = 3.75, Z_{28} =$

TABLE VI. Vibrational-rotational bound states $-E_{vJ}$ (in cm^{-1}) of the beryllium dimer. For each J in upper line MEMO* and in lower line STO* with relativistic corrections.

J	$v=0$	1	2	3	4	5	6	7	8	9	10	11
0	806.0	583.5	408.7	288.3	211.1	154.1	107.1	68.3	37.8	16.3	4.4	0.3
0	807.7	584.1	409.4	288.3	211.9	155.4	108.3	69.5	39.0	17.5	5.0	0.4
1	804.8	582.4	407.7	287.5	210.4	153.5	106.6	67.8	37.4	16.0	4.2	0.2
1	806.5	583.0	408.4	287.5	211.2	154.8	107.7	69.0	38.6	17.2	4.8	0.3
2	802.4	580.1	405.7	285.8	209.0	152.3	105.5	66.9	36.6	15.4	3.8	0.1
2	804.0	580.8	406.4	285.8	209.8	153.5	106.7	68.1	37.8	16.6	4.4	0.1
3	798.7	576.7	402.6	283.2	206.9	150.4	103.8	65.5	35.4	14.5	3.2	
3	800.4	577.4	403.5	283.3	207.7	151.7	105.1	66.7	36.7	15.7	3.8	
4	793.9	572.2	398.6	279.8	204.1	148.0	101.7	63.6	33.8	13.3	2.4	
4	795.5	573.0	399.5	279.9	204.9	149.3	102.9	64.8	35.1	14.5	3.0	
5	787.8	566.5	393.6	275.6	200.5	144.9	99.0	61.2	31.8	11.8	1.5	
5	789.5	567.4	394.5	275.8	201.5	146.3	100.2	62.5	33.2	13.0	2.1	
6	780.5	559.7	387.5	270.6	196.3	141.2	95.7	58.4	29.5	10.0	0.5	
6	782.2	560.7	388.6	270.8	197.3	142.6	97.0	59.7	30.9	11.2	1.0	
7	772.1	551.8	380.5	264.7	191.4	137.0	92.0	55.2	26.8	8.1		
7	773.7	552.9	381.7	265.0	192.5	138.4	93.3	56.5	28.2	9.2		
8	762.4	542.8	372.5	258.0	185.9	132.1	87.7	51.5	23.8	5.9		
8	764.1	544.0	373.8	258.4	187.0	133.6	89.1	52.9	25.2	7.0		
9	751.5	532.7	363.5	250.5	179.7	126.7	83.0	47.4	20.5	3.5		
9	753.2	534.0	364.9	251.0	180.9	128.3	84.4	48.8	21.9	4.6		
10	739.4	521.4	353.6	242.2	172.8	120.7	77.7	42.9	16.8	1.0		
10	741.1	522.9	355.1	242.8	174.2	122.4	79.2	44.3	18.3	2.0		

25] a.u. which corresponds to $r \in [r_1 = 1.9843, r_{28} = 13.229]$. One can see that these tabular values were chosen to provide the best approximation of the potential $V(r)$ by the fourth-order LIPs of the variable r in subintervals $r \in [r_{4k-3}, r_{4k+1}]$, $k = 1, \ldots, 6$. On interval $Z \in [Z_{25}, Z_{match} = 27.5]$ a.u. we consider the approximation of the potential $V(r)$ by the fifth-order HIP using the values of the potential $V(Z)$ at the points $Z = \{Z_{25} = 17.5, Z_{26} = 20.0, Z_{27} = 22.5, Z_{28} = 25.0\}$ a.u. and the values of the asymptotic potential $V_{as}(r)$ and its derivative $dV_{as}(Z)/dZ = s_3 dV_{as}(r)/dr$ at the point $Z = Z_{match} = 27.5$ a.u. In the interval $r \in [r_{match} = 14.552, \infty)$ the potential $V_{as}(r) = s_2 U_{as}(r)$ is approximated by the asymptotic expansion

$$U_{as}(r) = s_1 \tilde{V}_{as}(r), \quad \tilde{V}_{as}(r) = \tilde{V}_{as}^{BO}(r) + \tilde{V}_{as}^{rel}(r), \tag{6}$$
$$\tilde{V}_{as}^{rel}(r) = -\left(1.839 \cdot 10^{-4} Z^{-4} + 0.11944 Z^{-6} + 19.582 Z^{-8} - 1323.5 Z^{-10}\right),$$

where $\tilde{V}_{as}^{BO}(r)$ and $\tilde{V}_{as}^{rel}(r)$ are given by Eq. (5) and Ref.[19], respectively. The STO PEC constructed in such a way was called STO*. Note that using a similar behavior of MEMO and STO potential functions on the interval $r \in [12, 14]$ one can use also Eq. (6) for matching MEMO potential in interval $r \in [14, \infty)$, because it has been calculated taken into account the relativistic effects[30–32].

For comparison we show in Figure 3b the potential function $V(r)$, its asymptotic expansion $V_{as}(r)$ and the analytical potential functions $V_{an}(r)$ in a.u. (converted into cm^{-1}), proposed in Ref.[44]. The approximated MEMO* potential function $V(r)$ has a minimum $-D_e(\text{MEMO}^*) = V(r_e) = -929.804$ cm^{-1} at the equilibrium point $r_e = 2.4534$ Å, which is higher than the analytical potential function $V_{an}(r)$ in the vicinity of this point, $-D_e(\text{Sheng}) = V_{an}(r_e) = -948.3$ cm^{-1}. On the contrary, in the interval $r \in (3.2, 6.1)$ the analytical potential function $V_{an}(r)$ is greater than $V(r)$. For $r \in (2.3, 12)$, the MEMO potential slightly exceeds the STO one, which, in turn, is a bit higher than the MLR and CPE potentials. Thus, using the accepted approximations we have the MEMO and STO potential functions $V(r)$ approximated in the analytical form in interval $r \in (1.9, 14)$ and its smooth continuation at $r \geq 14$ by means of the asymptotic expressions (5) and (6).

TABLE VII. Vibrational-rotational bound states $-E_{vJ}$ (in cm^{-1}) of the beryllium dimer. For each J in upper line MEMO* and in lower line STO* with relativistic corrections. Continuation of Table VI.

J	$v=0$	1	2	3	4	5	6	7	8
11	726.2	509.1	342.6	233.2	165.3	114.2	72.0	38.0	12.9
11	727.9	510.7	344.4	233.9	166.8	115.9	73.6	39.5	14.4
12	711.7	495.6	330.8	223.4	157.2	107.1	65.8	32.8	8.7
12	713.4	497.4	332.7	224.3	158.8	108.9	67.4	34.3	10.2
13	696.0	481.1	318.0	212.9	148.5	99.5	59.2	27.1	4.4
13	697.8	483.1	320.1	213.9	150.2	101.4	60.9	28.7	5.9
14	679.2	465.5	304.3	201.7	139.2	91.4	52.2	21.2	−
14	681.0	467.7	306.6	202.8	141.0	93.4	53.9	22.9	1.4
15	661.2	448.8	289.7	189.8	129.3	82.8	44.7	15.0	
15	663.0	451.2	292.2	191.1	131.3	84.8	46.5	16.7	
16	642.1	431.0	274.2	177.3	118.9	73.8	36.9	8.5	
16	643.8	433.7	276.9	178.7	121.1	75.9	38.8	10.3	
17	621.8	412.2	257.9	164.2	108.0	64.3	28.7	1.9	
17	623.5	415.1	260.8	165.8	110.3	66.5	30.7	3.7	
18	600.3	392.4	240.7	150.4	96.6	54.4	20.3		
18	602.1	395.5	243.8	152.2	99.0	56.6	22.3		
19	577.7	371.5	222.8	136.2	84.8	44.1	11.5		
19	579.4	374.9	226.0	138.2	87.3	46.4	13.6		
20	553.9	349.7	204.0	121.5	72.5	33.5	2.6		
20	555.7	353.3	207.5	123.7	75.2	35.9	4.8		

TABLE VIII. Vibrational-rotational bound states $-E_{vJ}$ (in cm^{-1}) of the beryllium dimer. For each J in upper line MEMO* and in lower line STO* with relativistic corrections. Continuation of Table VI.

J	$v=0$	1	2	3	4	5	J	$v=0$	1	2
21	529.1	326.8	184.6	106.3	59.8	22.5	29	290.8	111.0	10.7
21	530.8	330.7	188.2	108.7	62.6	25.0	29	292.7	117.0	14.9
22	503.1	303.0	164.4	90.8	46.8	11.4	30	256.3	80.4	
22	504.9	307.2	168.2	93.4	49.7	13.9	30	258.2	86.6	
23	476.0	278.2	143.6	74.9	33.4	0.01	31	220.8	49.1	
23	477.8	282.7	147.6	77.8	36.4	2.5	31	222.7	55.6	
24	447.8	252.5	122.3	58.8	19.8		32	184.4	17.2	
24	449.6	257.2	126.4	61.9	22.9		32	186.3	23.9	
25	418.5	225.9	100.4	42.5	5.9		33	146.9		
25	420.3	230.9	104.7	45.8	9.1		33	148.9		
26	388.2	198.4	78.2	26.0			34	108.6		
26	390.0	203.7	82.5	29.6			34	110.6		
27	356.7	170.1	55.7	9.5			35	69.3		
27	358.6	175.6	60.1	13.3			35	71.4		
28	324.3	140.9	33.1				36	29.2		
28	326.1	146.7	37.5				36	31.3		

The MAPLE and FORTRAN programs used to get the analytical form of approximation for the MEMO[9] and STO[19] potential functions $V_J(r)$, respectively, extended over large intervals of internuclear distance r with the help of asymptotic expressions (5) and (6), are given in the supplementary material of Refs.[37,56]. Below we will use for these potential functions the following notations: MEMO* and STO*.

V. BOUND STATES OF THE BERYLLIUM DIMER

To calculate the vibrational-rotational spectrum of the real-valued eigenenergies E_{vJ} and corresponding eigenfunctions $\Phi_{vJ}(r)$ of the bound states of the beryllium dimer we solved the BVP for Eq. (3) using the FEM programs KANTBP 4M[53] and KANTBP 3.0[51] on the finite element mesh $\Omega_1(r) = \{1.9(0.1)2.4(0.05)2.8(0.1)4.0(0.2)5.0(0.5)8(2)20(5)40\}$, where the number in parentheses (x) is the size of subinterval, with the second-type or Neumann boundary conditions (BCs) on the boundary points of the mesh. In the BVP solution at all finite elements of the mesh the local functions were represented by fifth-order HIPs.

Table IV (columns MEMO* and STO*) presents the results of using FEM programs KANTBP 4M and KANTBP 3.0 to calculate 12 energy eigenvalues of the beryllium dimer. It shows the eigenvalues calculated with the MEMO potential function[9] and the corresponding approximation MEMO* from[37] and the previous Section IV. In contrast to the original EMO function, which was used to describe the experimental (Exp) vibrational levels[6], it has not only the correct dissociation energy, but also describes all twelve vibrational energy levels with the RMS error less than 0.4 cm^{-1}. The Table IV also shows the results of direct-potential-fit analysis using the MLR and CPE functions alongside with the EMO potential function[20], and CV+F+R potential function[14] discussed early in Section II. Similar results FCI/CBS+corr were obtained by Lesiuk et. al.[19] and STO* Derbov et. al.[37]. Their PEC lie below the MEMO one and also include the correct long-range behavior displayed in Figure 3. As a consequence, one can see from the Tables VI–VIII, that the corresponding results provide the theoretical *lower estimates* whereas MEMO* and MEMO results give the *upper estimates* for the discrete spectrum of the beryllium dimer at both $J = 0$ and $J > 0$ in accordance with[57]. One can see also that the STO* eigenenergies calculated using the STO* approximation of the tabulated PEC STO give smaller RMS error 0.7 cm^{-1} in comparison with RMS error 1.0 cm^{-1} of the FCI/CBS+corr eigenenergies calculated using the analytical fit of STO PEC[19].

The potential functions MEMO* and STO* $V_J(r)$ from $J = 0$ to $J = 36$ support 252 and 253 vibrational-rotational energy levels $-E_{vJ}$, respectively, presented in Tables VI–VIII. Figure 5a) (black dots) shows also the rotational-vibrational spectrum E_{vJ} (in cm^{-1}) of Be$_2$ vs J for MEMO* PEC. One can see that these potential functions $V_J(r)$ at $J = 0$, $J = 1$ and $J = 2$ support 12 vibrational energy levels and there is no energy level $E_{v=8,J=14}$ for MEMO* PEC.

Here and below the results presented in figures are calculated with MEMO* PEC.

VI. METASTABLE STATES OF THE BERYLLIUM DIMER

The BVP for Eq. (3) was solved using the FEM program KANTBP 5M[52] on the finite element mesh $\Omega_1(r) = \{1.9(0.1)2.4(0.05)2.8(0.1)20\}$ with the Neumann boundary conditions at the boundary point $r = r_{\min} = 1.90$ and the Robin boundary condition at the boundary point $r = r_{\max} = 20$ with logarithmic derivative for $\Phi_J(kr) \equiv \Phi_{Jv}^M(kr)$

$$\frac{d\Phi_J(kr)}{dr} - \mathscr{R}\Phi_J(kr) = 0, \quad \mathscr{R} = \frac{1}{\Phi_{as}^+(kr)}\frac{d\Phi_{as}^+(kr)}{dr}, \tag{7}$$

that followed from asymptotic solution for only the outgoing wave[54,58,59]

$$\Phi_{as}^+(kr) = \sqrt{k}h_J^{(1)}(kr) = -\iota\frac{\exp(+\iota(kr - \pi J/2))}{\sqrt{kr}} + O(k^{-3/2}r^{-2}). \tag{8}$$

Here complex-valued $k \equiv k_{Jv}^M = \sqrt{\mathscr{E}_{Jv}^M} = \sqrt{E_{Jv}^M/s_2}$ in units of Å^{-1} is the wave number, $E_{Jv}^M = s_2\mathscr{E}_{Jv}^M$ cm^{-1}, $h_J^{(1)}(z)$ is spherical Hankel function of the first kind[60].

The complex eigenenergies $E_{Jv}^M = \Re E_{Jv}^M + \iota\Im E_{Jv}^M$, (in cm^{-1}) of Be$_2$ rotational-vibrational metastable states, where v is the state number at a fixed value of J, are shown in Tables IX–XI. Their real parts

TABLE IX. The rotational-vibrational metastable states $E_{Jv}^M = \Re E_{Jv}^M + \iota \Im E_{Jv}^M$ (in cm^{-1}) of Be$_2$, where "eps" means that $-10^{-5} < \Im E_{Jv}^M < 0$ (in cm^{-1}). From left to right MEMO* and STO* with relativistic corrections. V_J^{min} and V_J^{max} are minimal and maximum values of potentials $V_J(r)$ (in cm^{-1}) at different values J of the total angular momentum. The metastable states with real part of energy $\Re E_{Jv}^M$ greater then the top of potential barrier V_J^{max} are marked by asterisk.

J	v	MEMO*		STO*		MEMO*		STO*	
		V_J^{min}	V_J^{max}	V_J^{min}	V_J^{max}	$\Re E$	$-\Im E$	$\Re E$	$-\Im E$
0		-929.80	0.00	-934.39	0.00				
1		-928.55	0.01	-933.15	0.01				
2		-926.07	0.04	-930.66	0.04				
3	11	-922.34	0.12	-926.92	0.11	0.081	0.010		
*4	11	-917.37	0.23	-921.93	0.24	0.281	0.101	0.256	0.063
5		-911.16	0.42	-915.70	0.43				
6		-903.71	0.71	-908.22	0.71				
7	10	-895.03	1.11	-899.59	1.09	0.503	6.1e-4	0.118	eps
8	10	-885.11	1.62	-889.52	1.57	1.509	0.090	1.254	0.026
*9	10	-873.95	2.24	-878.41	2.18			2.327	0.246
10		-861.57	3.00	-866.00	2.92				
11	9	-847.96	3.92	-852.36	3.82	1.554	1.3e-5	0.641	eps
12	9	-833.12	5.02	-837.49	5.04	4.052	0.030	3.308	3.8e-3
*13	9	-817.06	6.27	-821.41	6.27	6.356	0.321	5.788	0.152
14	8	-799.78	7.73	-804.11	7.64	0.083	eps		
*14	9	-799.78	7.73	-804.11	7.64			8.135	0.688
15	8	-781.28	9.39	-785.60	9.18	4.605	1.5e-5	3.126	eps
16	8	-761.57	11.26	-765.89	10.94	8.992	0.018	7.651	2.2e-3
17	8	-740.65	13.34	-744.97	12.94	13.016	0.314	11.896	0.124
18	7	-718.53	15.66	-722.85	15.19	4.788	eps	2.916	eps
*18	8	-718.53	15.66	-722.85	15.19			15.816	0.722
19	7	-695.21	18.22	-699.54	17.69	11.517	1.4e-4	9.635	eps
20	7	-670.68	21.05	-675.04	20.44	17.991	0.036	16.196	8.2e-3
21	6	-645.00	24.16	-649.36	23.45	6.403	eps	4.200	eps
21	7	-645.00	24.16	-649.36	23.45	23.915	0.481	22.276	0.230
22	6	-618.13	27.55	-622.51	26.73	15.497	eps	13.264	eps
23	6	-590.09	31.24	-594.48	30.30	24.444	3.7e-3	22.218	7.5e-4

$\Re E_{Jv}^M$ in comparison with the eigenenergies E_{vJ} of vibrational-rotational bound states are displayed in Figure 5a) (empty circles). This set of metastable states is supported by the potential functions $V_J(r)$ at $J = 3, 4, 7, 8, 9, 11, \ldots, 49$. Note that the real parts of energies $\Re E_{Jv}^M$ of the metastable states marked by an asterisk in Tables IX–XI lie above the top V_J^{max} of the potential barrier $V_J(r)$. Note that the bound state with energy $E_{v=8, J=14} = -1.44$ cm^{-1} for STO* PEC corresponds to the sharp metastable state for MEMO* PEC with complex energy $E_{J=14, v=8}^M = (0.083 - \iota 3 \cdot 10^{-29})$ cm^{-1}.

For $J > 0$, the potential functions at large r decrease proportionally to r^{-2} and at $J \leq 38$ they have the form of a potential well with a minimum below the dissociation threshold D_0, while at $J > 38$ the potential well has a minimum above the dissociation threshold. The height of the centrifugal barrier increases with increasing J, but its width at the dissociation threshold energy ($E = 0$) is infinite. With increasing energy, the effective width of the barrier decreases. The number of metastable states δv at $J \leq 38$ is determined by the number of positive-energy states in the potential well with the barrier of height V_J^{max} taken into account, i.e., in the well with the potential $V_J^* = \{V(r), r < r_{max}; V_{max}, r \geq r_{max}\}$. For small $J < 16$, the barrier height V_J^{max} counted from the zero energy is smaller than the energy difference between two upper levels of metastable states. This means that even one metastable state can exist not for all values of J. With the growth of J to $J = 33$, the barrier height increases, but the width of the well changes insignificantly.

TABLE X. The rotational-vibrational metastable states $E_{Jv}^M = \Re E_{Jv}^M + \imath \Im E_{Jv}^M$ (in cm^{-1}) of Be$_2$, where "eps" means that $-10^{-5} < \Im E_{Jv}^M < 0$ (in cm^{-1}). The metastable states with real part of energy $\Re E_{Jv}^M$ greater then the top of potential barrier $V_J^{\max}$ are marked by asterisk. Continuation of Table IX.

J	v	MEMO*		STO*		MEMO*		STO*	
		$V_J^{\min}$	$V_J^{\max}$	$V_J^{\min}$	$V_J^{\max}$	$\Re E$	$-\Im E$	$\Re E$	$-\Im E$
24	5	-560.92	35.25	-565.29	34.17	11.484	eps	8.853	eps
24	6	-560.92	35.25	-565.29	34.17	32.872	0.168	30.741	0.073
25	5	-531.76	39.58	-534.93	38.36	22.998	eps	20.324	eps
*25	6	-531.76	39.58	-534.93	38.36	40.609	1.155	38.526	0.764
26	4	-500.63	44.26	-503.43	42.90	7.996	eps	4.773	eps
26	5	-500.63	44.26	-503.43	42.90	34.354	1.4e-3	31.669	3.2e-4
27	4	-468.31	49.30	-470.77	47.80	22.032	eps	18.779	eps
27	5	-468.31	49.30	-470.77	47.80	45.187	0.100	42.578	0.044
28	3	-434.84	54.73	-436.96	53.00	6.963	eps	3.009	eps
28	4	-434.84	54.73	-436.96	53.00	35.991	eps	32.731	eps
*28	5	-434.78	54.73	-436.96	53.00	55.158	0.963	52.604	0.633
29	3	-400.28	60.57	-402.02	58.57	23.517	eps	19.452	eps
29	4	-400.28	60.57	-402.02	58.57	49.669	3.0e-4	46.445	8.5e-4
30	2	-364.63	66.91	-365.94	64.70	11.354	eps	7.180	eps
30	3	-364.63	66.91	-365.94	64.70	40.058	eps	35.968	eps
30	4	-364.63	66.91	-365.94	64.70	62.639	0.155	59.549	0.076
31	2	-327.89	73.60	-328.74	71.30	32.621	eps	28.549	eps
31	3	-327.89	73.60	-328.74	71.30	56.534	1.6e-4	52.550	3.0e-5
*31	4	-327.89	73.60	-328.74	71.30	74.626	1.306	71.589	0.939
32	2	-290.09	80.68	-290.41	78.37	52.660	eps	48.671	eps
32	3	-290.09	80.68	-290.41	78.37	72.662	0.030	68.982	0.011
33	1	-251.24	88.21	-250.96	85.94	15.028	eps	8.238	eps
33	2	-251.24	88.21	-250.96	85.94	71.131	2.4e-4	67.206	7.1e-5
33	3	-251.24	88.21	-250.96	85.94	87.630	0.696	84.364	0.476
34	1	-211.35	96.30	-210.39	94.04	47.644	eps	40.779	eps
34	2	-211.35	96.30	-210.39	94.04	87.890	0.026	84.078	0.012
35	1	-170.43	105.04	-168.75	102.73	80.254	eps	73.432	eps
35	2	-170.43	105.04	-168.75	102.73	102.939	0.414	99.326	0.266
36	1	-128.50	124.02	-125.94	120.39	111.593	0.057	105.389	6.8e-3

As a result, the number of metastable states increases to three. With further increase in J, when in the interval $r \in (3.5, 6)$ the slope of centrifugal potential exceeds the slope of MEMO* potential, the well width rapidly decreases, so that only two states can exist in the well, a bound state and a metastable one at $J = 36$ and two metastable states at $J = 34, 35, 37, 38$. At $J \geq 39$ the potential well minimum turns to be above the dissociation threshold ($E = 0$) and the effective barrier width, the width and depth of the well decrease. Only one state exists in the well, its width increasing with the growth of J. At $J > 49$ there are no energy levels in the well, and at $J > 54$ the potential well disappears.

As can be seen from Tables IX–XI and Figures 6, 7, the eigenfunctions of metastable states with complex energy values for a fixed value of the orbital momentum J have an increasing number of nodes localized inside the potential well. Beginning from each lower state above the dissociation threshold, they have one node more than the last bound state with real energy under the dissociation threshold ($E = 0$) with the same value of the orbital momentum J in Tables VI–VIII. Thus, there is a continuation of the theoretical *upper and lower estimates* of the real energy eigenvalues E_{Jv} to the complex plane $E_{Jv}^M = \Re E_{Jv}^M + \imath \Im E_{Jv}^M$, labeled by the number of nodes v of eigenfunctions localized inside the potential well, for each value of the orbital momentum J.

TABLE XI. The rotational-vibrational metastable states $E_{Jv}^M = \Re E_{Jv}^M + \iota \Im E_{Jv}^M$ (in cm^{-1}) of Be$_2$, where "eps" means that $-10^{-5} < \Im E_{Jv}^M < 0$ (in cm^{-1}). The metastable states with real part of energy $\Re E_{Jv}^M$ greater then the top of potential barrier $V_J^{\max}$ are marked by asterisk. Continuation of Table X.

J v	MEMO*		STO*		MEMO*		STO*	
	$V_J^{\min}$	$V_J^{\max}$	$V_J^{\min}$	$V_J^{\max}$	$\Re E$	$-\Im E$	$\Re E$	$-\Im E$
37 0	-85.58	147.94	-83.10	144.01	11.780	eps	9.538	eps
37 1	-85.58	147.94	-83.10	144.01	144.261	3.272	137.920	2.408
38 0	-41.68	173.18	-38.98	168.91	53.590	eps	51.233	eps
*38 1	-41.68	173.18	-38.98	168.91	177.154	6.591	170.793	5.797
39 0	3.17	199.73	6.08	195.12	96.169	eps	93.672	eps
40 0	48.96	227.57	52.02	222.65	139.466	eps	136.795	eps
41 0	95.66	256.70	98.82	251.52	183.406	8.3e-4	180.520	1.2e-3
42 0	143.26	287.15	146.44	281.76	227.880	0.023	224.726	0.030
43 0	191.72	318.91	194.85	313.39	272.755	0.148	269.266	0.175
44 0	241.01	352.03	244.03	346.07	317.922	0.544	314.022	0.625
45 0	291.11	386.52	293.90	379.47	363.371	1.432	358.983	1.622
46 0	341.98	422.41	344.47	413.61	409.201	3.008	404.261	3.371
*47 0	393.56	459.75	395.60	448.50	455.552	5.372	450.005	5.993
*48 0	445.83	498.57	447.31	487.87	502.577	8.560	496.339	9.508
*49 0	498.71	538.92	499.48	528.37	550.248	12.903		

VII.   SCATTERING STATES OF THE BERYLLIUM DIMER

The scattering problem for Eq. (3) at real-valued $E > 0$ in cm^{-1} was solved using the FEM programs KANTBP 5M[52] on the finite element mesh $\Omega_1(r) = \{1.9(0.1)2.4(0.05)2.8(0.1)20\}$. The eigenfunctions $\Phi_J(kr)$ of the scattering states are subjected to the Neumann boundary conditions (BCs) at the boundary point $r = r_{\min} = 1.90$ and the Robin boundary condition at the boundary point $r = r_{\max} = 20$ formulated as follows:

$$\frac{d\Phi_J(kr)}{dr} = \frac{d\Phi_{as}^J(kr)}{dr}, \quad \Phi_J(kr) = \Phi_{as}^J(kr), \tag{9}$$

at $r = r_{\max}$ using the asymptotic form 'incident wave + outgoing wave'[60]

$$\Phi_{as}^J(kr) = \frac{\iota^J}{\sqrt{2\pi}}(\Phi_{as}^-(kr) + \Phi_{as}^+(kr)S_J(E)). \tag{10}$$

Here $S_J(E) = \exp(2\iota\delta_J(E))$ is the partial scattering matrix, and the outgoing wave $\Phi_{as}^+(kr)$ and incident wave $\Phi_{as}^-(kr) = (\Phi_{as}^+(kr))^*$ functions are given by (8) at real-valued $k = \sqrt{\mathscr{E}} = \sqrt{E/s_2} > 0$ in units of Å^{-1}, where * denotes the complex-conjugation.

Plots of the real (solid curves) and imaginary (dashed curves) parts of scattering functions in the vicinity of the resonance energy for the narrow resonance at $J = 12$ and very narrow resonance at $J = 18$ are shown in Figure 8. One can see that the resonant scattering functions are localized in the potential well, which is no longer observed upon a minor change in the energy of the incident wave. As can be seen from Tables IX–XI, the energies of resonant states $E(res)$ are close to the real parts of the energies $\Re E_{Jv}^M$ of metastable states. In particular, for $J = 12$ $E(res) \approx 4.043$ cm^{-1} and for $J = 18$ $E(res) \approx 4.789$ cm^{-1} are close to $\Re E_{J=12v=9} = 4.052$ cm^{-1} and $\Re E_{J=18v=7} = 4.788$ cm^{-1}, respectively.

In Figure 9, the corresponding phase shifts δ vs the scattering energy E are shown; as expected, the phase shifts take the value $\delta = \pi/2$ for resonance energies and change rapidly in their vicinity. To estimate the scattering length a_0 of the scattering state at $k \to 0$ we apply the formula[60]

$$a_0 = -\lim_{k \to 0} \frac{\tan \delta_0(k)}{k} \approx -\frac{d\delta_0(k)}{dk}\bigg|_{k \to 0}.$$

The recalculated value a_0 at $k \to 0$ provides an *upper estimate* for the scattering length $a_0 = 6.55$ Å.

Since the MEMO* potential gives the *upper bound*, and the STO* potential gives the *lower bound* energy of twelfth state (see Table IV), the calculation with the STO* potential leads to the *lower bound* for the scattering length $a_0 = 3.31$ Å, as well as for EMO ($a_0 = 4.87$ Å), MLR ($a_0 = 0.91$ Å) and CPE ($a_0 = 0.77$ Å) potentials[20].

VIII. CONCLUSIONS

The present study shows that the beryllium atoms are covalently bound in Be_2 at the low-lying vibrational energy levels with $v = 0 - 4$, while at the higher levels with $v = 5 - 11$ the atoms are bonded by the van der Waals forces near the right turning points. The EMO potential energy function used in the experimental research[6] for fitting the measured vibrational energy levels of Be_2 does not correctly describe this dual nature of the chemical bonding. It describes better the covalent bonding on the low-lying vibrational energy levels than the van der Waals bonding on the upper ones. A comparison of the EMO potential energy function with the potential function obtained in the high precision *ab initio* calculation carried out in the present study shows that the EMO function is too narrow near the dissociation limit. Therefore, the modified EMO potential function has been constructed by replacing the parts of the original EMO function near dissociation limit and above it by the *ab initio* potential function. The obtained MEMO potential function not only has the correct dissociation energy, but, in distinction with EMO potential function, also describes all twelve vibrational energy levels with a smaller RMS error of less than 0.4 cm^{-1}.

Special attention in this study was payed on improved calculations of spectrum of the bound vibrational-rotational state together with spectrum of the metastable vibrational-rotational state having complex-valued eigenenergies. The existence of these metastable states is confirmed by calculation of the corresponding scattering states with real values of the resonance energies. Theoretical *upper and lower estimates* are of significant importance for further experiments in laser spectroscopy of the beryllium dimer. It is also important for modeling of a near-surface diffusion of the beryllium dimers[61–66] in connection with the well-known multifunctional use of beryllium alloys in modern technologies of the electronic, space and nuclear industries[67], and, in particular, the ITER project[68].

IX. ACKNOWLEDGEMENTS

X. REFERENCES

[1] J. H. J. Bartlett and W. H. Furry, "Valence forces in Lithium and Beryllium," Phys. Rev. **38**, 1615–1622 (1931).

[2] I. Roeggen and J. Almlöf, "Interatomic potential for the $X^1\Sigma_g^+$ state of Be_2," Int. J. Quantum Chem. **60**, 453–466 (1996).

[3] W. A. Shirley and G. A. Petersson, "Comment: The convergence of coupled-cluster methods for Be_2," Chem. Phys. Lett. **181**, 588–590 (1991).

[4] L. Füsti-Molnar and P. Szalay, "High-quality theoretical potential energy surface for Be_2 by using the multireference everaged quadratic coupled-cluster (MR-AQCC) method and large basis sets," Chem. Phys. Lett. **258**, 400–408 (1996).

[5] J. Stärk and W. Meyer, "The ground state potential of the beryllium dimer," Chem. Phys. Lett. **258**, 421–426 (1996).

[6] J. M. Merritt, V. E. Bondybey, and M. C. Heaven, "Beryllium Dimer - Caught in the Act of Bonding," Science **324**, 1548–1551 (2009).

[7] A. V. Mitin, "Ab initio calculations of weakly bonded He_2 and Be_2 molecules by MRCI method with pseudo-natural molecular orbitals," Int. J. Quantum Chem. **111**, 2560–2567 (2011).

[8] R. T. Birge and H. Sponer, "The heat of dissociation of non-polar molecules," Phys. Rev. **28**, 259–283 (1926).

[9] A. V. Mitin, "Unusual chemical bonding in the beryllium dimer and its twelve vibrational levels," Chem. Phys. Lett. **682**, 30–33 (2017).

[10] I. Røggen and L. Veseth, "Interatomic potential for the $X^1\Sigma_g^+$ state of Be_2, revisited," Int. J. Quantum Chem. **101**, 201–210 (2005).

[11] K. Patkowski, R. Podeszwa, and K. Szalewicz, "Interactions in diatomic dimers involving closed-shell metals," J. Phys. Chem. A **111**, 12822–12838 (2007).

[12] K. Patkowski, V. Špirko, and K. Szalewicz, "On the elusive twelfth vibrational state of beryllium dimer," Science **326**, 1382–1384 (2009).

[13] M. W. Schmidt, J. Ivanic, and K. Ruedenberg, "Electronic Structure Analysis of the Ground-State Potential Energy Curve of Be_2," J. Phys. Chem. A **114**, 8687–8696 (2010).

[14] J. Koput, "The ground-state potential energy function of a beryllium dimer determined using the single-reference coupled-cluster approach," Phys. Chem. Chem. Phys. **13**, 20311–20317 (2011).

[15] S. Sharma, T. Yanai, G. H. Booth, C. J. Umrigar, and G. K.-L. Chan, "Spectroscopic accuracy directly from quantum chemistry: Application to ground and excited states of beryllium dimer," J. Chem. Phys. **140**, 104112 (2014).

[16] M. Lesiuk, M. Przybytek, M. Musiał, B. Jeziorski, and R. Moszynski, "Reexamination of the calculation of two-center, two-electron integrals over Slater-type orbitals. III. Case study of the beryllium dimer," Phys. Rev. A **91**, 012510 (2015).

[17] I. Magoulas, N. P. Bauman, J. Shen, and P. Piecuch, "Application of the CC(P;Q) Hierarchy of Coupled- Cluster Methods to the Beryllium Dimer," J. Phys. Chem. A **122**, 1350–1368 (2018).

[18] Z. Rolik and M. Kállay, "Novel strategy to implement active-space coupled-cluster methods," J. Chem. Phys. **148**, 124108 (2018).

[19] M. Lesiuk, M. Przybytek, J. G. Balcerzak, M. Musiał, and R. Moszynski, "Ab initio Potential Energy Curve for the Ground State of Beryllium Dimer," J. Chem. Theor. Comput. **15**, 2470–2480 (2019).

[20] V. V. Meshkov, A. V. Stolyarov, M. C. Heaven, C. Haugen, and R. J. LeRoy, "Direct-potential-fit analyses yield improved empirical potentials for the ground $X^1\Sigma_g^+$ state of Be_2," J. Chem. Phys. **140**, 064315 (2014).

[21] J. A. Coxon and P. G. Hajigeorgiou, "Isotopic dependence of born-oppenheimer breakdown effects in diatomic hydrides: The $B^1\Sigma^+$ and $X^1\Sigma^+$ states of HCl and DCl," J. Mol. Spectr. **139**, 84–106 (1990).

[22] A. V. Mitin, "Calculation of rotational-vibrational energy levels of diatomic molecules by the Dunham method with ab initio potential," Zh. Fiz. Khim. **64**, 2041–2044 (1990).

[23] A. V. Mitin, "Calculation of the rovibrational energy levels of diatomic molecules by the Dunham method with a potential obtained from ab initio calculations," J. Comput. Chem. **19**, 94–101 (1998).

[24] A. G. Gaydon, "The determination of dissociation energies by the birge-sponer extrapolation," Proc. Phys. Soc. **58**, 525–538 (1946).

[25] A. V. Mitin, "Iterative methods for calculations of extreme eigenvalues of large symmetric matrices," Mathematical Modelling and Geometry **2**, 10–26 (2014).

[26] R. D. Amos, A. Bernhardsson, A. Berning, P. Celani, D. L. Cooper, M. J. O. Deegan, A. J. Dobbyn, F. Eckert, C. Hampel, G. Hetzer, P. J. Knowles, T. Korona, R. Lindh, A. W. Lloyd, S. J. McNicholas, F. R. Manby, W. Meyer, M. E. Mura, A. Nicklass, P. Palmieri, R. Pitzer, G. Rauhut, M. Schütz, U. Schumann, H. Stoll, A. J. Stone, R. Tarroni, T. Thorsteinsson, and H.-J. Werner, *MOLPRO, version 2002.6. A Package of Ab Initio Programs* (Birmingham, UK, 2003).

[27] T. H. Dunning, "Gaussian basis sets for use in correlated molecular calculations. I. The atoms boron through heon and hydrogen," J. Chem. Phys. **90**, 1007–1023 (1989).

[28] R. A. Kendall, T. H. Dunning, and R. J. Harrison, "Electron affinities of the first-row atoms revisited. Systematic basis sets and wave functions," J. Chem. Phys. **96**, 6796–6806 (1992).

[29] D. E. Woon and T. H. Dunning, "Gaussian basis sets for use in correlated molecular calculations. IV. Calculation of static electrical response properties," J. Chem. Phys. **100**, 2975–2988 (1994).

[30] M. Douglas and N. M. Kroll, "Quantum electrodynamical corrections to the fine structure of helium," Annals of Physics **82**, 89–155 (1974).

[31] B. A. Hess, "Applicability of the no-pair equation with free-particle projection operators to atomic and molecular structure calculations," Phys. Rev. A **32**, 756–763 (1985).

[32] B. A. Hess, "Relativistic electronic-structure calculations employing a two-component no-pair formalism with external-field projection operators," Phys. Rev. A **33**, 3742–3748 (1986).

[33] S. F. Boys and F. Bernardi, "The calculation of small molecular interactions by the differences of separate total energies. some procedures with reduced errors," Mol. Phys. **19**, 553–566 (1970).

[34] F. B. van Duijneveldt, J. G. C. M. van Duijneveldt-van de Rijdt, and J. H. van Lenthe, "State of the art in counterpoise theory," Chem. Rev. **94**, 1873–1885 (1994).

[35] R. J. Gdanitz, "Accurately solving the electronic Schrödinger equation of atoms and molecules by extrapolating to the basis set limit. I. The helium dimer (He_2)," J. Chem. Phys. **113**, 5145–5153 (2000).

[36] G. A. Petersson and W. A. Shirley, "The beryllium dimer potential," Chem. Phys. Lett. **160**, 494–501 (1989).

[37] V. Derbov, G. Chuluunbaatar, A. Gusev, O. Chuluunbaatar, S. Vinitsky, A. Góźdź, P. Krassovitskiy, I. Filikhin, and A. Mitin, "Spectrum of beryllium dimer in ground $X^1\Sigma_g^+$ state," J. Quant. Spectrosc. Radiat. Transf. **262**, 107529 (2021).

[38] R. J. Gdanitz, "Accurately solving the electronic schrödinger equation of atoms and molecules using explicitly correlated (r_{12}-)MR-CI. the ground state of beryllium dimer (Be_2)," Chem. Phys. Lett. **312**, 578–584 (1999).

[39] J. L. Dunham, "The Wentzel-Brillouin-Kramers Method of Solving the Wave Equation," Phys, Rev. **41**, 713–720 (1932).

[40] J. L. Dunham, "The Energy Levels of a Rotating Vibrator," Phys, Rev. **41**, 721–731 (1932).

[41] A. V. Mitin, "New methods for solution of electron equations of quantum chemistry and its applications," Doctor thesis, Moscow, Moscow State University (2013).

[42] P. M. Morse, "Diatomic molecules according to the wave mechanics. II. Vibrational levels," Phys. Rev. **34**, 57–64 (1929).

[43] S. Porsev and A. Derevianko, "High-accuracy calculations of dipole, quadrupole, and octupole electric dynamic polarizabilities and van der Waals coefficients C_6, C_8, and C_{10} for alkaline-earth dimers," J. Exp. Theor. Phys. **102**, 195–205 (2006).

[44] X. W. Sheng, X. Y. Kuang, P. Li, and K. T. Tang, "Analyzing and modeling the interaction potential of the ground-state beryllium dimer," Phys. Rev. A **88**, 022517 (2013).

[45] B. M. Smirnov, *Cluster Ions and Van Der Waals Molecules* (Gordon and Breach Sience Publisher S A, Amsterdam, 1992).

[46] S. R. Patil and K. T. Tang, *Asymptotic methods in quantum mechanics. Application to atoms, molecules and nuclei* (Springer-Verlag, Berlin Heidelberg, 2000).

[47] J. Jiang, J. Mitroy, Y. Chengb, and M.W.J.Bromley, "Effective oscillator strength distributions of spherically symmetric atoms for calculating polarizabilities and long–range atom–atom interactions," Atomic Data and Nuclear Data Tables **101**, 158–186 (2015).

[48] A. Gusev, O. Chuluunbaatar, S. Vinitsky, V. Derbov, A. Góźdź, L. Hai, and V. Rostovtsev, "Symbolic-numerical solution of boundary-value problems with self-adjoint second-order differential equation using the finite element method with interpolation Hermite polynomials," Lecture Notes in Computer Science **8660**, 138–154 (2014).

[49] A. Gusev, O. Chuluunbaatar, S. Vinitsky, V. Derbov, A. Góźdź, P. Krassovitskiy, I. Filikhin, A. Mitin, L. Hai, and T. Lua, "On rotational-vibrational spectrum of diatomic beryllium molecule," Proc. SPIE **11066**, 1106619 (2019).

[50] V. Derbov, G. Chuluunbaatar, A. Gusev, O. Chuluunbaatar, S. Vinitsky, A. Góźdź, P. Krassovitskiy, and A. Mitin, "On calculations of metastable and rydberg states of diatomic beryllium molecule and antiprotonic helium atom," Proc. SPIE **11458**, 114580Q (2020).

[51] A. Gusev, O. Chuluunbaatar, S. Vinitsky, and A. Abrashkevich, "Kantbp 3.0: New version of a program for computing energy levels, reflection and transmission matrices, and corresponding wave functions in the coupled-channel adiabatic approach," Comput. Phys. Commun. **185**, 3341–3343 (2014).

[52] G. Chuluunbaatar, A. Gusev, V. Derbov, S. Vinitsky, L. Hai, O. Chuluunbaatar, and V. Gerdt, "A maple implementation of the finite element method for solving boundary-value problems for systems of second-order ordinary differential equations," Maple Conference 2020 **1414**, 152–166 (2021).

[53] A. Gusev, O. Chuluunbaatar, S. Vinitsky, and L. Hai, "KANTBP 4M - program for solving boundary problems of the self-adjoint system of ordinary second order differential equations," JINRLIB, http://wwwinfo.jinr.ru/programs/jinrlib/kantbp4m (2015), accessed: 2023-03-29.

[54] A. Gusev, L. Hai, O. Chuluunbaatar, V. Ulziibayar, S. Vinitsky, V. Derbov, A. Góźdź, and V. Rostovtsev, "Symbolic-numeric solution of boundary-value problems for the Schrödinger equation using the finite element method: scattering problem and resonance states," Lect. Notes Computer Sci. **9301**, 182–197 (2015).

[55] "Atomic spectroscopy databases," https://www.nist.gov/pml/atomic-spectroscopy-databases (2009), accessed: 2023-03-29.

[56] "Supplementary material associated with paper[37]," https://10.1016/j.jqsrt.2021.107529 (2021).

[57] R. Courant and D. Hilbert, *Methods of Mathematical Physics, Vol. 1* (Wiley-VCH).

[58] V. I. Kukulin, V. M. Krasnopolsky, and J. Horráček, *Theory of Resonances: Principles and Applications* ((Reidel Texts Math. Sci., Vol. 3),Springer, Netherlands, 1989).

[59] A. J. F. Siegert, "On the derivation of the dispersion formula for nuclear reactions," Phys. Rev. **56**, 750–752 (1939).

[60] M. Goldberger and K. Watson, *Collision Theory* (John Wiley, New York, 1964).

[61] P. M. Krassovitskiy and F. M. Pen'kov, "Contribution of resonance tunneling of molecule to physical observables," J. Phys. B: At. Mol. Opt. Phys. **47**, 225210 (2014).

[62] A. Gusev, S. Vinitsky, O. Chuluunbaatar, A. Góźdź, and V. Derbov, "Resonance tunnelling of clusters through repulsive barriers," Physica Scripta **89**, 054011 (2014).

[63] S. I. Vinitsky, A. A. Gusev, O. Chuluunbaatar, L. L. Hai, V. L. Derbov, P. M. Krassovitskiy, and A.Góźdź, "Symbolic numerical algorithm for solving quantum tunneling problem of a diatomic molecule through repulsive barriers," Lecture Notes in Computer Science **8660**, 472–490 (2014).

[64] A. A. Gusev, S. I. Vinitsky, O. Chuluunbaatar, V. L. Derbov, A. Góźdź, and P. M. Krassovitskiy, "Metastable states of a composite system tunneling through repulsive barriers," Theoretical and Mathematical Physics **186**, 21–40 (2016).

[65] A. Gusev, S. Vinitsky, O. Chuluunbaatar, V. Derbov, A. Góźdź, and P. Krassovitskiy, "Transmission of clusters consisting of a few identical particles through barriers and wells," Acta Physica Polonica B Proceedings Supplement **10**, 269–274 (2017).

[66] A. A. Gusev, S. I. Vinitsky, O. Chuluunbaatar, A. Góźdź, V. L. Derbov, and P. M. Krassovitskiy, "Adiabatic representation for atomic dimers and trimers in collinear configuration," Phys. Atom. Nucl. **81**, 945–970 (2018).

[67] K. A. Walsh, *Beryllium chemistry and processing* (ASM International, Ohio, 2009).

[68] A. Allouche and C. Linsmeier, "Quantum study of tungsten interaction with beryllium (0001)," J. Phys. Conf. Ser. **117**, 012002 (2008).
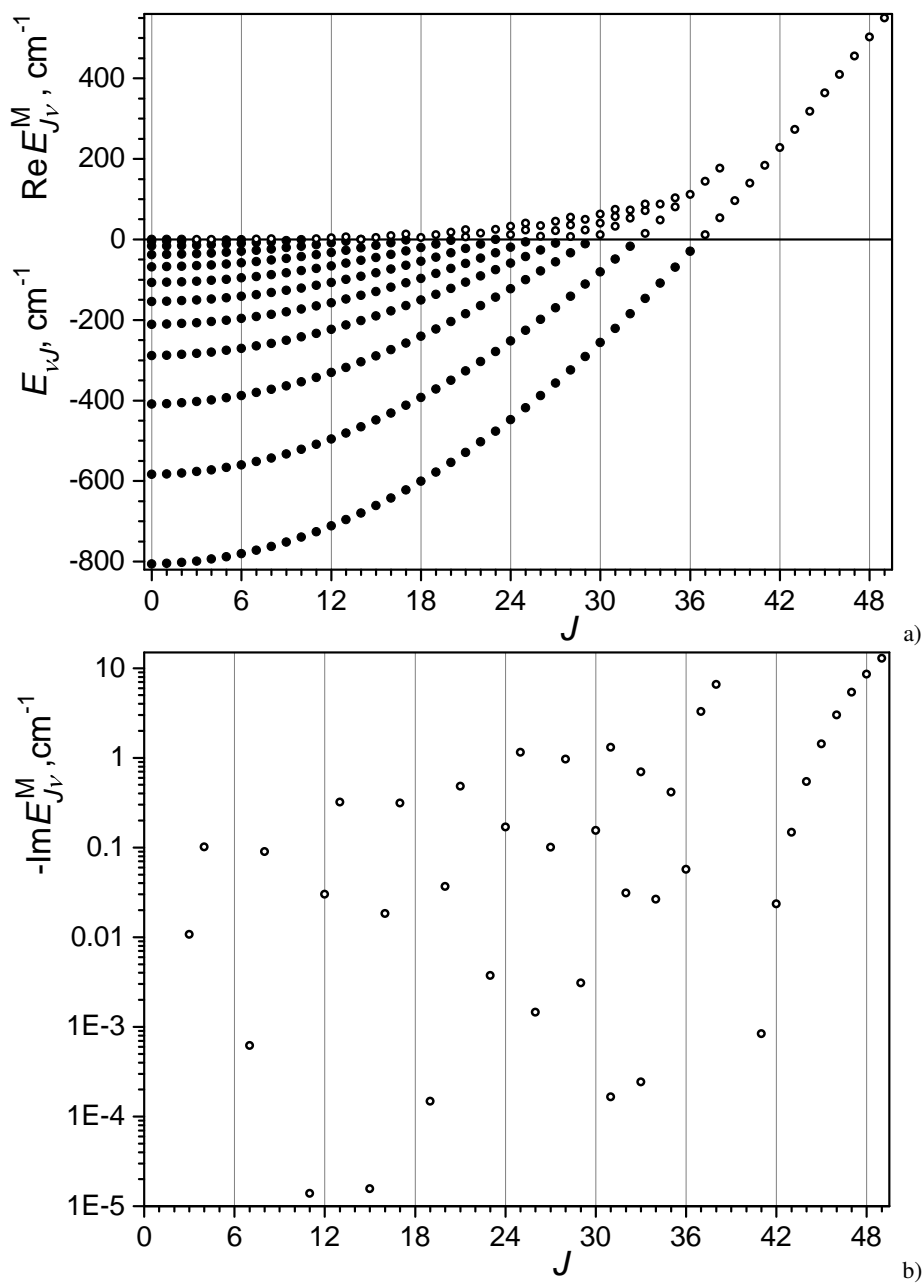
FIG. 5. a) Eigenenergies E_{vJ} of vibrational-rotational bound states (black dots), the real part $\Re E_{Jv}^M$ (empty circles) and b) minus the imaginary part $-\Im E_{Jv}^M$ of complex eigenenergies $E_{Jv}^M = \Re E_{Jv}^M + \imath \Im E_{Jv}^M$ of rotational-vibrational metastable states in cm^{-1}.
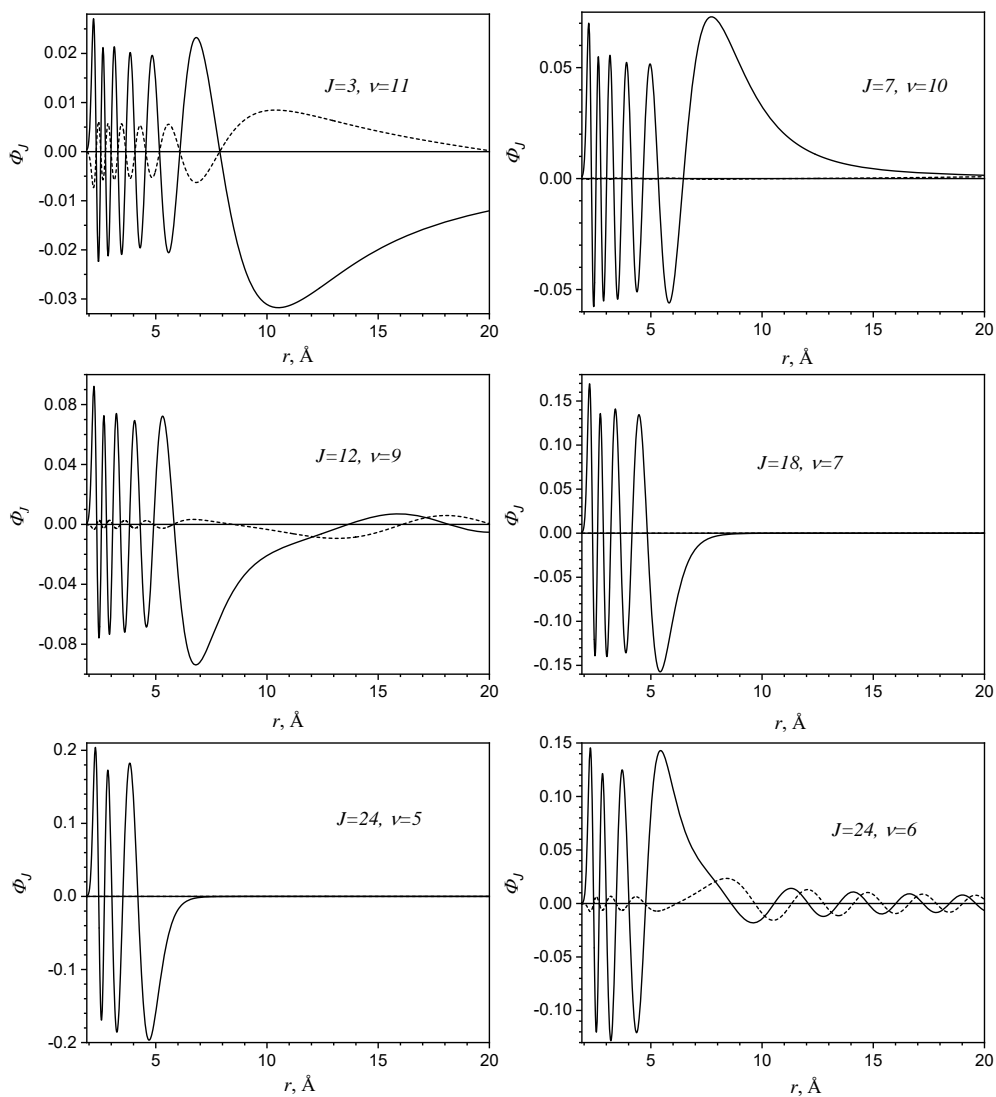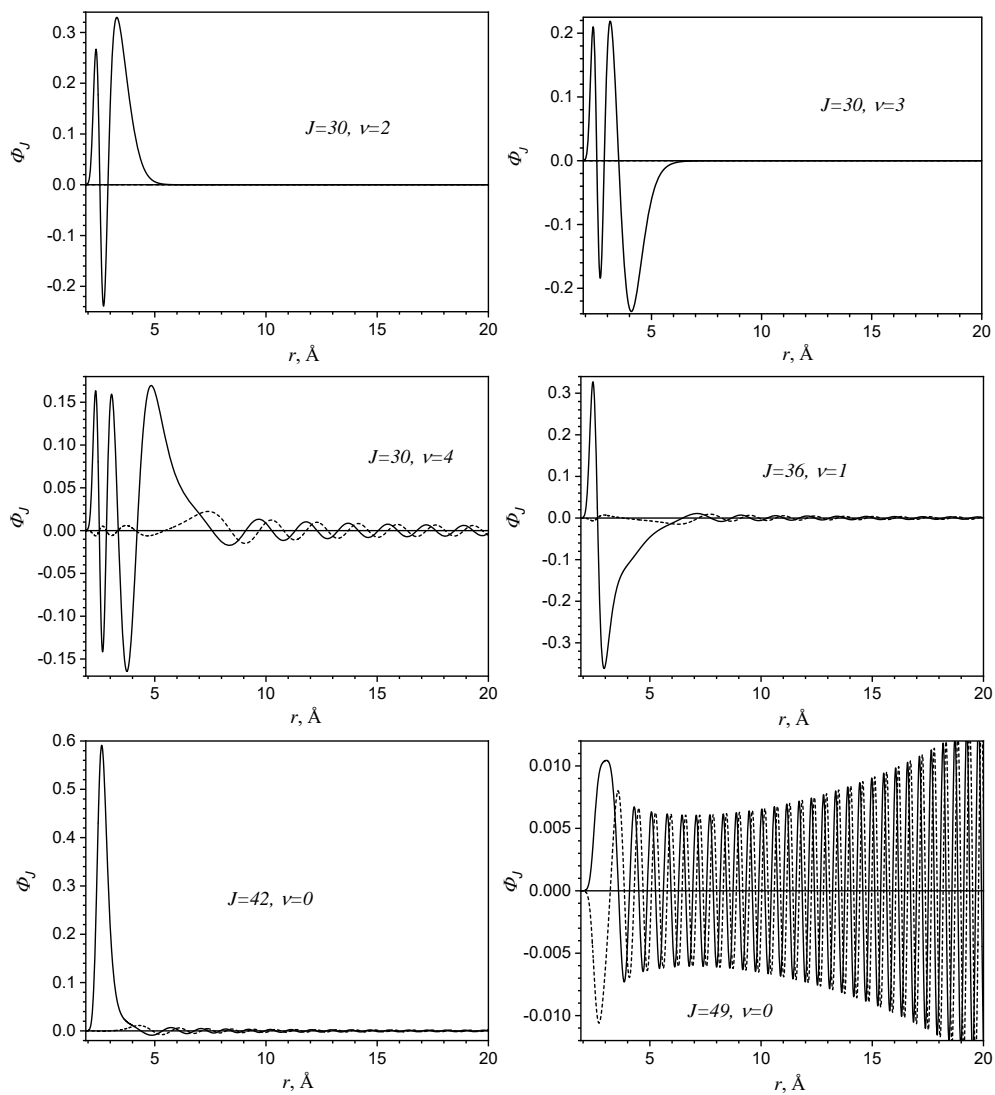
FIG. 6. Plots of real (solid curve) and imaginary (dashed curve) parts of eigenfunctions $\Phi_{J\nu}^{M}(r)$ of selected metastable states having eigenvalues from the Tables IX and X marked by $J = 3, 7, 12, 18, 24$ and ν.

FIG. 7. Plots of real (solid curve) and imaginary (dashed curve) parts of eigenfunctions $\Phi_{J\nu}^{M}(r)$ of selected metastable states having eigenvalues from the Tables X and XI marked by $J =$ 30, 36, 42, 49 and ν.
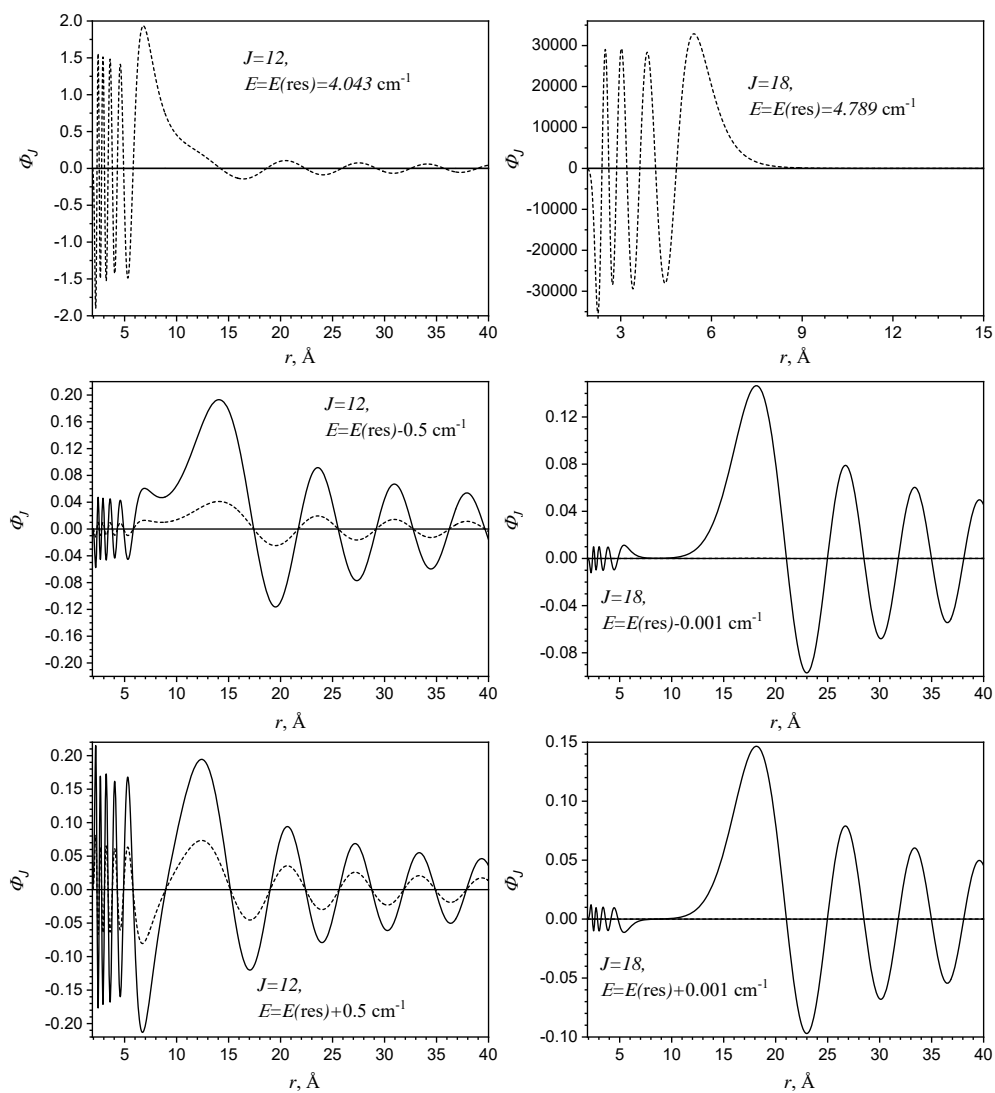
FIG. 8. Plots of the real (solid curves) and imaginary (dashed curves) parts of scattering wave functions $\Phi_J \equiv \Phi_J(r)$ in the vicinity of the resonance energy $E(res)$ at $J = 12$ and $J = 18$.
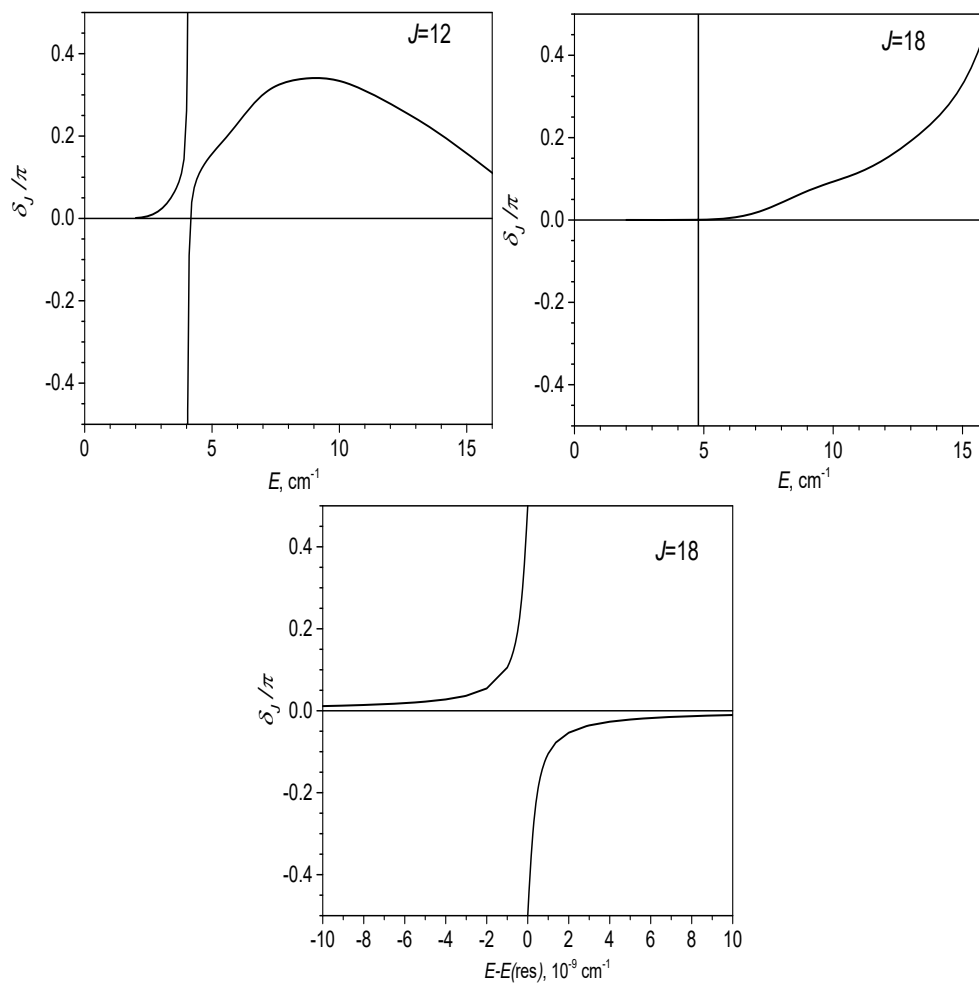
FIG. 9. Phase shifts δ_J vs scattering energy E counted from $E = 0$ at $J = 12$ and $J = 18$.